

Stoch-IDENT: New Method and Mathematical Analysis for Identifying SPDEs from Data

Jianbo Cui, Roy Y. He

Abstract

In this paper, we propose Stoch-IDENT, a novel method for identifying Stochastic Partial Differential Equations (SPDEs) from observational data. Our method can handle linear and nonlinear high-order SPDEs driven by time-dependent Wiener processes with both additive or multiplicative structures. Theoretically, we establish a rigorous connection between the spectral properties of the solution’s mean and covariance and the identifiability of the underlying SPDEs. Our analysis covers key classes of equations, including linear SPDEs with constant coefficients, as well as parabolic and hyperbolic types, generalizing the theory of identification of deterministic PDEs. Algorithmically, the drift term is identified using a sample mean generalization of Robust-IDENT (He et al., 2023). For the diffusion term, we develop a new greedy algorithm, Quadratic Subspace Pursuit (QSP), which can address general sparse regression problems with quadratic measurements. We validate Stoch-IDENT extensively on various SPDEs, demonstrating its effectiveness through quantitative and qualitative evaluations.

1 Introduction

Data-driven discovery of Partial Differential Equations (PDEs) has been catching extensive attention since PDE-FIND [48] and IDENT [37]. Generalizing the sparsity-inducing regression framework initiated by Brunton et al. [10], these PDE identification algorithms find the differential operators that compose the models which govern the dynamical behaviors of the observational data, yielding valuable techniques for model discovery in biological sciences [23], geosciences [50], and oceanography [20].

Various advancements have been developed to address diverse application problems involving PDEs [44, 6, 60, 59]. To mitigate noise amplification caused by numerical differentiation and overcome model redundancy, Robust-IDENT [33] was introduced. This framework employs an ℓ_0 -constraint formulation, efficiently solved using the Subspace Pursuit (SP) algorithm [18]. Due to its effectiveness, the framework has been widely adopted in recent PDE identification methods, including Weak-IDENT [54] for integral-form PDEs, CaSLR [34] for patch-based PDE identification, Fourier-IDENT [55] for identification in the frequency domain, GP-IDENT [32] and WG-IDENT [53] for PDEs with varying coefficients, and its integral-form variation. A comprehensive review can be found in [31]. Additionally, deep learning-based approaches, such as those in [41, 22, 51], offer alternative solutions.

The pervasive presence of stochasticity, whether inherent or external, in system dynamics necessitates different paradigms. Consequently, there is increasing interest in data-driven identification of stochastic differential equations (SDEs) to enable accurate uncertainty modeling and enhance predictive analysis. Most existing works focus on stochastic Ordinary Differential Equation (ODE) or systems. For example, Boninsegna et al. extended SINDy to stochastic dynamical systems using the Kramers-Moyal formulae [8]. Wang et al. proposed a sparse Bayesian learning framework for systematically discovering parsimonious SDE forms. Tripura et al. [56] also developed a Bayesian framework with sparsity induced by a spike-and-slab (SS) prior, employing Gibbs sampling to draw from the joint distribution of model parameters. Beyond Gaussian noise, generalizations to non-Gaussian Lévy-type noise were explored in [39]. To the best of our knowledge, the work by Mathpati et al. [43] is the first study addressing data-driven identification of Stochastic Partial Differential Equations (SPDEs). They extended the Kramers-Moyal expansion and applied the SS prior for sparsity while finding the model terms via a variational Bayesian framework using the Kullback–Leibler (KL) divergence. More recently, Tipura et al. [57] considered generalizing their framework with tailored dictionaries suitable for identifying Hamiltonian and Lagrangian of physical systems. Gerardos and Ronceray [27] introduced

Parsimonious Stochastic Inference (PASTIS) as a better metric than Akaike’s Information Criterion (AIC) which has been adopted in SINDy-based methods for model selection.

Notably, the aforementioned methods for SPDE identification are primarily based on the Kramers-Moyal expansion and focus on identifying the *squared* diffusion part rather than the diffusion part itself. Indeed, recovering the latter, whether in a pathwise or an expectation sense, requires nonlinear regression. This is a more challenging procedure that has not been addressed in previous work. Furthermore, although these methods have been validated on various nonlinear and high-order SPDEs, their applicability to SPDEs with multiplicative noise remains underexplored in the existing literature.

Another critical yet unresolved issue is the theoretical understanding of when and why SPDEs can be uniquely identified from data. For deterministic PDEs, He et al. [34] established a foundational theory, demonstrating that the identifiability of a PDE depends on the dimension of its solution space. Their work reveals why parabolic PDEs are inherently more challenging to identify than hyperbolic ones. In the specific case of linear PDEs with constant coefficients, they further proved that just two time snapshots of the solution trajectory suffice for unique identification, provided the initial condition contains sufficiently rich Fourier modes. However, extending these results to SPDEs is non-trivial. The stochasticity introduces new complexities, necessitating a different analytical framework.

In this work, we address these challenges through both algorithmic and theoretical advancements. Specifically, we propose **Stoch-IDENT**, a novel framework for identifying SPDEs from path sample data. Our approach is capable of handling both linear and nonlinear high-order SPDEs driven by time-dependent Wiener processes with both additive or multiplicative structures. Different from existing methods based on the Kramers-Moyal expansion and Bayesian framework, we exploit the formulation of ℓ_0 -constrained sparse regression. For the drift term identification, we reduce the problem to deterministic PDE identification by taking path expectations, enabling us to leverage the computational efficiency of Robust-IDENT [33] through a sample mean generalization. The diffusion term identification is formulated as an ℓ_0 -constrained sparse regression problem with quadratic measurements [24]. To address this combinatorially complex nonlinear problem, we develop **Quadratic Subspace Pursuit (QSP)** (Algorithm 1), a new greedy algorithm that extends the expansion-shrinking paradigm [32] of SP [18] to nonlinear regression. Unlike deterministic settings, the identified SPDE coefficients are random variables due to sample average approximations. We establish theoretical guarantees by proving the asymptotic convergence of these sample-based solutions. Extensive numerical experiments across various SPDEs demonstrate the effectiveness of our approach.

On the theoretical side, we present a comprehensive identifiability analysis for linear SPDEs with constant coefficients. When the driving noise is independent of the solution (additive noise case), we show that the drift term is identifiable in average sense, provided that the expectation of the initial data contains sufficiently many nontrivial Fourier modes. In contrast, with the multiplicative noise (the noise term depends on the solution itself), unique identification requires rich Fourier modes of initial data almost surely. With regard to the diffusion identification, we utilize the covariance structure of stochastic integrals, which enables us to determine the diffusion terms uniquely up to equivalence classes, thus providing a robust framework for operator recovery even in the presence of stochasticity. Note that once the pathwise information of stochastic integral is given, unique identification of the diffusion operators in the classical sense is available.

Furthermore, we analyze the data space spanned by solution trajectories of three types of SPDEs: parabolic, hyperbolic and Schrödinger equation. For the parabolic case, we find that the data space can be approximated to accuracy $\mathcal{O}(\epsilon)$ by a linear space of dimension $\mathcal{O}(|\log(\epsilon)|)^2$ in the averaged sense (see subsection 3.2.1). While in the hyperbolic case, via the stochastic characteristics, we obtain the similar approximation result as in the deterministic case [34] (see subsection 3.2.2). Most intriguingly, for the stochastic Schrödinger equation, we find that the data space spanned by the average of the solution trajectory can be approximated by the linear space of logarithmic dimension (see subsection 3.2.3), whereas the data space spanned by the solution itself only admits polynomial-dimensional approximation.

To summarize, our contributions in this paper include

1. A novel framework, Stoch-IDENT, for identifying SPDEs driven by time-dependent Wiener processes with both additive and multiplicative structures. The proposed method is both computationally efficient and effective at finding the underlying drift and diffusion terms based on samples from multiple paths.
2. For identifying the diffusion terms, we design a new greedy algorithm, Quadratic Subspace

Pursuit (QSP), for the associated sparse regression problems with quadratic measurements. The proposed algorithm can be applicable to more general problems such as phase retrieval.

3. An in-depth mathematical analysis on the identifiability of SPDEs. For linear SPDEs with constant coefficients, our theory establishes precise conditions under which both drift and diffusion terms can be uniquely identified. For parabolic and hyperbolic SPDEs and stochastic Schrödinger equation, we analyze the dimensions of data spaces spanned by the respective solution trajectories, generalizing the theory for deterministic PDEs in [34].
4. Extensive numerical experiments for testing the proposed Stoch-IDENT across various SPDEs with both additive and multiplicative noises.

This paper is organized as follows. In Section 2, we provide an overview of our proposed framework for identifying SPDEs from data Stoch-IDENT. In Section 3, we analyze the identifiability conditions for linear SPDEs with constant coefficients, including parabolic, hyperbolic, and stochastic Schrödinger equations. In Section 4, we discuss the major components of Stoch-IDENT and propose our algorithm Quadratic Subspace Pursuit (QSP). In Section 5, we discuss more details in the implementation, which can enhance the identification performances. In Section 6, we present numerical results to validate our method and theory. We conclude this paper in Section 7.

2 Proposed Method: Stoch-IDENT

In this section, we present **Stoch-IDENT**, a method for identifying SPDEs from observed data. The method finds an SPDE whose strong solutions approximate the observed trajectories. We provide a high-level overview of the framework here, while deferring detailed algorithmic steps to Section 4.

2.1 Mathematical formulation of the problem

Let $\mathcal{U} = \{U_n : \Gamma \rightarrow \mathbb{R}\}_{n=1}^N$ be a collection of observed trajectories, where Γ is a grid on the observation time-space domain $[0, T] \times \mathcal{D} \subset \mathbb{R} \times \mathbb{R}^d$, $d \geq 1$ is the space dimension, and N is the number of trajectories. We assume that each U_n can be approximated by a strong solution of an unknown SPDE driven by a time-dependent Wiener process W in the following form

$$du = \sum_{k=1}^K a_k F_k dt + \sum_{j=1}^J b_j G_j dW(t), \quad (1)$$

with some appropriate boundary conditions. In the generic form (1), the drift term is a linear combination of K *candidate drift features* $\{F_k : [0, T] \times \mathcal{D} \rightarrow \mathbb{R}\}_{k=1}^K$, each of which is assumed to be a monomial of partial derivatives of u with respect to the space, e.g., u_{xx} or uu_x ; and the diffusion term is a linear combination of J *candidate diffusion features* $\{G_j : [0, T] \times \mathcal{D} \rightarrow \mathbb{R}\}_{j=1}^J$, which are also monomials of spatial derivatives of u . For $k = 1, 2, \dots, K$, we call $a_k \in \mathbb{R}$ the feature coefficient of the k -th drift feature; and for $j = 1, 2, \dots, J$, we call $b_j \in \mathbb{R}$ the feature coefficient of the j -th diffusion feature. When $a_k = 0$ for some k , we say that the k -th drift feature is inactive; otherwise we say that it is active. This is similarly defined for the diffusion features.

The solution approximation by the observed trajectories is understood in the *pathwise sense*. More precisely, let $(\Omega, \mathcal{F}, (\mathcal{F})_{t \geq 0}, \mathbb{P})$ be the filtered probability space where (1) is defined, $\Gamma = \{(t_i, x_m) : i = 0, 1, \dots, I, m = 0, 1, \dots, M\}$ be the set of grid points, $\{\omega_n\}_{n=1}^N$ be N samples from Ω , and $u_n := u(\omega_n) : [0, T] \times \mathcal{D}$ be a strong solution of (1) driven by a sample path of Wiener process $W(t, \omega_n)$. For $n = 1, 2, \dots, N$, the trajectory U_n is obtained by sampling the solution:

$$U_n(t_i, x_m) = u_n(t_i, x_m), \quad i = 0, 1, \dots, I; m = 0, 1, \dots, M. \quad (2)$$

Our objective is to identify the active drift and diffusion features and recover the corresponding feature coefficients based on the observed data. The above framework can be easily adapted to identifying SDE or stochastic systems; for more details on such extensions, we refer the readers to [37, 33, 54].

2.2 Overview of the proposed Stoch-IDENT framework

Suppose the underlying SPDE can be represented by the generic form (1), i.e., the set of candidate drift and diffusion features is complete. We propose to identify the active features by the following steps:

Step 1. Identify the drift features from sample means. Leveraging the martingale property of the stochastic integral, the diffusion part of (1) can be eliminated by considering its expectation. Consequently, we first search for the active drift features and estimate the associated coefficients by exploiting the relation:

$$d\mathbb{E}[u] = \sum_{k=1}^K a_k \mathbb{E}[F_k] dt. \quad (3)$$

To ensure interpretability and capture only important features, we require that only a few features are active, i.e., (a_1, \dots, a_K) is sparse. This task can be addressed by IDENT [37], Robust-IDENT [33], or PDE-FIND [48], and we explain the details in Section 4.

Step 2. Identify the diffusion features from squared drift residuals. To find the diffusion features and the associated coefficients b_j , we consider the following relation:

$$\mathbb{E} \left[\left(u(t_{i+1}, x) - u(t_i, x) - \int_{t_i}^{t_{i+1}} \sum_{k=1}^K a_k F_k(t, x) dt \right)^2 \right] = \mathbb{E} \left[\left(\int_{t_i}^{t_{i+1}} \sum_{j=1}^J b_j G_j(t, x) dW(t) \right)^2 \right]. \quad (4)$$

for any $x \in \mathcal{D}$ and $i = 1, \dots, I$, where $t_1 < t_2 < \dots < t_I$ is a sequence of times in $[0, T]$. If the estimates $\{\hat{a}_k\}_{k=1}^K$ obtained from Step 1 are close to the true coefficients $\{a_k\}_{k=1}^K$, we expect that (4) holds approximately after replacing a_k with \hat{a}_k for $k = 1, \dots, K$. Note that (4) is quadratic in $\{b_j\}_{j=1}^J$, whereas (3) is only linear in $\{a_k\}_{k=1}^K$. This is challenging especially when sparsity is desired. For this, we propose a novel algorithm in Section 4.

After obtaining the drift coefficient estimation $\hat{\mathbf{a}} = (\hat{a}_1, \dots, \hat{a}_K) \in \mathbb{R}^K$ from (3) and the diffusion coefficient estimation $\hat{\mathbf{b}} = (\hat{b}_1, \dots, \hat{b}_J) \in \mathbb{R}^J$ from (4), the identified SDE is expressed as

$$du = \sum_{k=1}^K \hat{a}_k F_k dt + \sum_{j=1}^J \hat{b}_j G_j dW_t. \quad (5)$$

If the identified model (5) is well-posed, by (3) and (4), we expect that if $\hat{\mathbf{a}}$ and $\hat{\mathbf{b}}$ are close to $\mathbf{a} = (a_1, \dots, a_K)$ and $\mathbf{b} = (b_1, \dots, b_J)$ respectively, then increments of solutions of (1) and (5) have similar means and variances.

Remark 2.1. *If the underlying SPDE is linear, and the terms are correctly identified with accurately estimated coefficients, then the well-posedness of (5) is standard. The nonlinear cases are more delicate. For example, under suitable boundary and initial conditions, the following parabolic SPDE*

$$du = \Delta u dt - \varepsilon u^3 dt + d\widetilde{W}(t)$$

is globally well-posed; whereas the equation

$$du = \Delta u dt + \varepsilon u^3 dt + d\widetilde{W}(t)$$

is only locally well-posed where $\varepsilon > 0$ is a constant and $\widetilde{W}(\cdot) = \sum_{i \in \mathbb{N}} Q^{\frac{1}{2}} e_i d\beta_i(\cdot)$ is a Q -Wiener process [40]. Here $Q^{\frac{1}{2}}$ is the square root of covariance operator of \widetilde{W}_t and $\{e_i\}_{i \in \mathbb{N}}$ is an orthonormal basis of Hilbert space L^2 . This implies that to keep the well-posedness of the original problem, the signs of the identified drift terms should be the same. Consider another example:

$$du = \Delta u dt - u^3 dt + a u^2 d\widetilde{W}(t)$$

under suitable boundary and initial conditions, with a constant $a \neq 0$. By applying the Itô's formula to $\|u(t)\|^2$, it can be seen that a sufficient condition such that $u \in L^2$ globally is

$$-2\|\nabla u\|_{L^2}^2 - 2\|u\|_{L^4}^4 + a^2 \sum_{i \in \mathbb{N}} \int_{\mathcal{D}} |u|^4 |Q^{\frac{1}{2}} e_i|^2 dx \leq c(1 + \|u\|_{L^2}^2)$$

for some constant $c \geq 0$. Note that different absolute value of a will affect the global well-posedness of SPDE. This implies that to keep the well-posedness of original problem, one should also assume more properties of the solutions for the identified SPDEs.

3 Identifiability Analysis of Stoch-IDENT

In this section, we analyze the mathematical properties of Stoch-IDENT. In particular, we are interested in when can a SPDE be uniquely determined by its strong solution based on the relations (3) and (4). Throughout this work, the driving Wiener process W is considered to be only time-dependent. It should be noticed that our theoretical framework can also be extended to the case that the driving process is space-time dependent, i.e., $W(t, x) = \sum_{l=1}^{\tilde{N}} R_l(x) \beta_l(t)$, $\tilde{N} \in \mathbb{N}^+ \cup \{+\infty\}$ with R_l being the real-valued functions, β_l being independent Brownian motions on $(\Omega, \mathcal{F}, \{\mathcal{F}_t\}_{t \geq 0}, \mathbb{P})$, and $\mathbb{N}^+ := \mathbb{N} \setminus \{0\}$. Let $\mathcal{D} = \mathbb{T}^d$ and denote $\widehat{f}(\xi), \xi \in \mathbb{Z}^d$, as the Fourier transformation of $f \in L^2(\mathcal{D})$, i.e.,

$$\widehat{f}(\xi) = (2\pi)^{-\frac{d}{2}} \int_{\mathcal{D}} e^{-i\xi \cdot x} f(x) dx ,$$

where $i^2 = -1$. Then we can apply the Fourier transformation on both sides of (1) and obtain the following

$$d\widehat{u}(\xi) = \sum_{k=1}^K a_k \widehat{F}_k(\xi) dt + \sum_{j=1}^J b_j \widehat{G}_j(\xi) dW(t) .$$

In this paper, we suppose that before some $T > 0$, the strong solution of (1) exists uniquely (see, e.g., [40, Appendix G]), i.e., there exists a unique \mathcal{F}_t -adapted stochastic process u such that

$$u(t) = u(0) + \int_0^t \sum_{k=1}^K a_k F_k ds + \int_0^t \sum_{j=1}^J b_j G_j dW(s), \text{ a.s. ,}$$

where the right-hand side is finite for any $t \in [0, T]$. Note that this definition also requires that $u(t)$ belong to the domain of every deterministic feature and to the domain of every stochastic feature, implying that $u(t)$ is \mathcal{F}_t -adaptive and satisfies

$$\int_0^T \mathbb{E} \sum_{j=1}^J b_j^2 \|G_j\|^2 dt < +\infty .$$

Here $\|\cdot\|$ is the L^2 -norm on the physical domain. Alternatively, we can consider SPDEs in the Stratonovich sense

$$du = \sum_{k=1}^K a_k F_k dt + \sum_{j=1}^J b_j G_j \circ dW(t) , \tag{6}$$

as it is also equivalent to a stochastic equation in the Itô sense (see e.g., [35, Chapter 7]). The advantage of using (6) is that it automatically admits the chain rule.

3.1 Linear SPDE identification with constant coefficient

We consider the identification problem related to linear SPDEs with constant coefficients. We show that the underlying differential operators \mathcal{L} and \mathcal{G} of SPDEs can be identified if the solution contains enough Fourier modes.

Consider the following linear SPDE,

$$du = \mathcal{L}u dt + \mathcal{G}R \circ dW(t) , \tag{7}$$

where $\mathcal{L} = \sum_{|\alpha|=0}^{p_1} a_\alpha \partial_x^\alpha$ is linear operator with constant coefficients and the total number of summands is K . The diffusion operator $\mathcal{G} = \sum_{|\beta|=0}^{p_2} b_\beta \partial_x^\beta$ with the number of summands J . Suppose that either R is a given real-valued function (additive noise case), or $R = u$ (multiplicative noise case). Here

the above stochastic integral is understood in the Stratonovich sense, and $\alpha, \beta \in \mathbb{N}^d$, $a_\alpha, b_\beta \in \mathbb{R}$, and $p_1, p_2 \in \mathbb{N}$.

By the Fourier transformation, one can get the corresponding system in the frequency space,

$$d\widehat{u}(t, \xi) = (2\pi)^{-\frac{d}{2}} \sum_{|\alpha|=0}^{p_1} a_\alpha(\mathbf{i}\xi)^\alpha \widehat{u}(t, \xi) dt + (2\pi)^{-\frac{d}{2}} \sum_{|\beta|=0}^{p_2} b_\beta(\mathbf{i}\xi)^\beta \widehat{R}(\xi) \circ dW(t). \quad (8)$$

Note that when R is independent of u , the Stratonovich integral above is equivalent to the Itô's integral [36]. The Duhamel principle further yields that for any $t_2 \geq t_1 \geq 0$

$$\begin{aligned} \widehat{u}(t_2, \xi) &= \widehat{u}(t_1, \xi) \exp \left((2\pi)^{-\frac{d}{2}} \sum_{|\alpha|=0}^{p_1} a_\alpha(\mathbf{i}\xi)^\alpha (t_2 - t_1) \right) \\ &\quad + (2\pi)^{-\frac{d}{2}} \sum_{|\beta|=0}^{p_2} b_\beta(\mathbf{i}\xi)^\beta \int_{t_1}^{t_2} \exp \left((2\pi)^{-\frac{d}{2}} \sum_{|\alpha|=0}^{p_1} a_\alpha(\mathbf{i}\xi)^\alpha (t_2 - s) \right) \widehat{R}(\xi) \circ dW(s). \end{aligned} \quad (9)$$

In particular, in the multiplicative noise case, by the chain rule we further have that

$$\frac{\widehat{u}(t_2, \xi)}{\widehat{u}(t_1, \xi)} = \exp \left((2\pi)^{-\frac{d}{2}} \sum_{|\alpha|=0}^{p_1} a_\alpha(\mathbf{i}\xi)^\alpha (t_2 - t_1) \right) \exp \left((2\pi)^{-\frac{d}{2}} \sum_{|\beta|=0}^{p_2} b_\beta(\mathbf{i}\xi)^\beta (W(t_2) - W(t_1)) \right). \quad (10)$$

Our idea of identification is firstly studying the drift terms via the average of sample trajectories. Then we study the diffusion identification through the covariance information of the stochastic integral.

3.1.1 Drift identification

The drift identification result is obtained via the property of conditional expectation.

Proposition 3.1. *Let $\mathcal{Q} = \{\xi \in \mathbb{Z}^d : \widehat{u}_0(\xi) \neq 0\}$ satisfy*

$$|\mathcal{Q}| \geq \max \left(\sum_{k=0}^{\lfloor \frac{p_1}{2} \rfloor} \binom{2k+d-1}{d-1}, \sum_{k=0}^{\lfloor \frac{p_1-1}{2} \rfloor} \binom{2k+d}{d} \right), a.s.$$

Suppose that \mathcal{Q} is not located in an algebraic polynomial hypersurface of degree $\leq p_1$ consisting of only even-order terms or odd-order terms a.s. Then the parameters $a_\alpha, |\alpha| \leq p_1$, are uniquely determined by the solution at two time points $u(t_1, \cdot), u(t_2, \cdot)$ if $|t_2 - t_1|$ is sufficiently small.

Proof. We only show the proof in the multiplicative noise case since that in additive noise case is similar. The main difference between the proofs in these two cases is that, for multiplicative noise, we begin by taking the expectation of (10), whereas for additive noise, we first take the expectation of (9). For completeness, we put it in the Appendix A.1.

For simplicity, we assume that $t_2 > t_1 = 0$. In the multiplicative noise case, by taking the polar coordinates on (10), for any $t_1 \neq t_2$, and $\widehat{u}(t_1, \xi) \neq 0$, it holds that

$$\begin{aligned} (2\pi)^{\frac{d}{2}} \log \left(\left| \frac{\widehat{u}(t_2, \xi)}{\widehat{u}(t_1, \xi)} \right| \right) &= \sum_{|\alpha| \leq p_1, \alpha \text{ even}} a_\alpha(\mathbf{i}\xi)^\alpha (t_2 - t_1) + \sum_{|\beta| \leq p_2, \beta \text{ even}} q_\beta(\mathbf{i}\xi)^\beta (W(t_2) - W(t_1)), \quad (11) \\ (2\pi)^{\frac{d}{2}} \text{Arg} \left(\left| \frac{\widehat{u}(t_2, \xi)}{\widehat{u}(t_1, \xi)} \right| \right) &= \sum_{|\alpha| \leq p_1, \alpha \text{ odd}} a_\alpha(\mathbf{i}\xi)^\alpha \mathbf{i}^{-1} (t_2 - t_1) + \sum_{|\beta| \leq p_2, \beta \text{ odd}} b_\beta(\mathbf{i}\xi)^\beta \mathbf{i}^{-1} (W(t_2) - W(t_1)). \end{aligned} \quad (12)$$

By taking expectation on (11)-(12), we have that

$$\frac{(2\pi)^{\frac{d}{2}}}{t_2 - t_1} \mathbb{E} \left[\log \left(\left| \frac{\widehat{u}(t_2, \xi)}{\widehat{u}(t_1, \xi)} \right| \right) \right] = \sum_{|\alpha| \leq p_1, \alpha \text{ even}} a_\alpha(\mathbf{i}\xi)^\alpha, \quad (13)$$

$$\frac{(2\pi)^{\frac{d}{2}}}{t_2 - t_1} \mathbb{E} \left[\text{Arg} \left(\left| \frac{\widehat{u}(t_2, \xi)}{\widehat{u}(t_1, \xi)} \right| \right) \right] = \sum_{|\alpha| \leq p_1, \alpha \text{ odd}} a_\alpha(\mathbf{i}\xi)^\alpha \mathbf{i}^{-1}. \quad (14)$$

Notice that for $|t_2 - t_1| > 0$ sufficiently small, the phase ambiguity in (12) can be removed.

We can choose the Fourier modes $\xi_k \in \mathcal{Q}$ with $k = 1, \dots, \tilde{K} \geq |\mathcal{Q}|$. Then we can rewrite (13) and (14) as

$$\frac{(2\pi)^{\frac{d}{2}}}{t_2 - t_1} \mathbf{y}_{\text{even}} = \mathbf{A}_{\text{even}} \mathbf{c}_{\text{even}}, \quad \frac{(2\pi)^{\frac{d}{2}}}{t_2 - t_1} \mathbf{y}_{\text{odd}} = \mathbf{A}_{\text{odd}} \mathbf{c}_{\text{odd}},$$

where $\mathbf{c}_{\text{even}}^\top = (\mathbf{i}^{|\alpha|} a_\alpha)_{|\alpha| \leq p_1, \text{even}}$, and $\mathbf{c}_{\text{odd}}^\top = (\mathbf{i}^{|\alpha|-1} a_\alpha)_{|\alpha| \leq p_1, \text{odd}}$. Here

$$(\mathbf{y}_{\text{even}})_k = \mathbb{E} \log \left(\left| \frac{\hat{u}(t_2, \xi_k)}{\hat{u}(t_1, \xi_k)} \right| \right), \quad (\mathbf{A}_{\text{even}})_{k\alpha} = \xi_k^\alpha, \quad |\alpha| \leq p_1 \text{ and is even},$$

$$(\mathbf{y}_{\text{odd}})_k = \mathbb{E} \text{Arg} \left(\left| \frac{\hat{u}(t_2, \xi_k)}{\hat{u}(t_1, \xi_k)} \right| \right), \quad (\mathbf{A}_{\text{odd}})_{k\alpha} = \xi_k^\alpha, \quad |\alpha| \leq p_1 \text{ and is odd}.$$

From the assumption on \mathcal{Q} , we have that \mathbf{A}_{even} and \mathbf{A}_{odd} are both of full ranks. This implies that a_α can be uniquely determined. \square

Once the drift terms are identified, we are now in a position to deal with diffusion identifications.

3.1.2 Diffusion identification

In this part, we present the diffusion identification result based on the covariance information of the corresponding stochastic integral. Since we did not assume any pathwise information of the stochastic convolution, our diffusion identification is unique in the sense of equivalent class (see e.g. (16)-(17)). Note that if the pathwise information of stochastic integral is known, then the unique identification is also available in classical sense (see detailed arguments in Appendix A.2). However, the accuracy of identified coefficient based on one sample trajectory may be quite low even though it may identify the correct terms in the dictionary.

Theorem 3.2. *Let $a_\alpha \in \mathbb{R}, |\alpha| \leq p_1$, be given. Let $\mathcal{Q}_1 = \{\xi \in \mathbb{Z}^d | \hat{R}(\xi) \neq 0\}$ in the additive noise case and $\mathcal{Q}_1 = \{\xi \in \mathbb{Z}^d | \mathbb{E} \hat{u}_0(\xi) \neq 0\}$ in the multiplicative noise case. Assume that $|\mathcal{Q}_1|$ is sufficiently large and that \mathcal{Q}_1 is not located on an algebraic polynomial hypersurface of degree $\leq 2p_1$. Then the parameters $b_\beta, |\beta| \leq p_2$, are uniquely determined, up to an equivalent class, by two instants $u(t_2, \cdot), u(t_1, \cdot)$ with $|t_2 - t_1| > 0$ sufficiently small.*

Proof. We only show the details in the multiplicative noise case, and put the proof for the additive noise case in Appendix A.3 for completeness. These proofs are similar. The main difference of these two proofs lies on the way to get the covariance information. In the multiplicative noise, we apply Itô's isometry and exponential moment equality to (10), while in the additive noise case, we directly use Itô's isometry to study the covariance of stochastic integral appearing in (9).

By the chain rule and the mild formulation of $\hat{u}(\xi, t)$, we have that for any $t_1 \neq t_2$, and $\hat{u}(t_1, \xi) \neq 0$,

$$\hat{u}(t_2, \xi) = \hat{u}(t_1, \xi) \exp \left((2\pi)^{-\frac{d}{2}} \sum_{|\alpha|=0}^{p_1} a_\alpha (\mathbf{i}\xi)^\alpha (t_2 - t_1) \right) \exp \left((2\pi)^{-\frac{d}{2}} \sum_{|\beta|=0}^{p_2} b_\beta (\mathbf{i}\xi)^\beta (W(t_2) - W(t_1)) \right).$$

Taking conditional expectation on the above equality, and using the independent increments of Brownian motion, it follows that

$$\frac{\mathbb{E} \hat{u}(t_2, \xi)}{\mathbb{E} \hat{u}(t_1, \xi)} = \exp \left((2\pi)^{-\frac{d}{2}} \sum_{|\alpha|=0}^{p_1} a_\alpha (\mathbf{i}\xi)^\alpha (t_2 - t_1) \right) \mathbb{E} \left[\exp \left((2\pi)^{-\frac{d}{2}} \sum_{|\beta|=0}^{p_2} b_\beta (\mathbf{i}\xi)^\beta (W(t_2) - W(t_1)) \right) \right].$$

According to the distribution of $W(t)$, we have the following exponential moment equality,

$$\mathbb{E}[e^{cW(t)}] = e^{\frac{c^2 t}{2}}, \quad \forall c \in \mathbb{C}. \quad (15)$$

This implies that

$$\frac{\mathbb{E} \hat{u}(t_2, \xi)}{\mathbb{E} \hat{u}(t_1, \xi)} = \exp \left((2\pi)^{-\frac{d}{2}} \sum_{|\alpha|=0}^{p_1} a_\alpha (\mathbf{i}\xi)^\alpha (t_2 - t_1) \right) \exp \left(\frac{1}{2} (2\pi)^{-d} \sum_{|\beta|, |\hat{\beta}|=0}^{p_2} b_\beta b_{\hat{\beta}} \mathbf{i}^{|\beta|+|\hat{\beta}|} \xi^{\beta+\hat{\beta}} (t_2 - t_1) \right).$$

Then by considering the polar coordinates, we obtain

$$(2\pi)^{\frac{d}{2}} \log \frac{\mathbb{E}\widehat{u}(t_2, \xi)}{\mathbb{E}\widehat{u}(t_1, \xi)} - \sum_{|\alpha| \text{ even}} a_\alpha (\mathbf{i}\xi)^\alpha (t_2 - t_1) = \frac{1}{2} \sum_{|\beta|+|\widehat{\beta}| \text{ even}}^{p_2} \mathbf{i}^{|\beta|+|\widehat{\beta}|} \xi^{\beta+\widehat{\beta}} b_\beta b_{\widehat{\beta}} (t_2 - t_1),$$

$$(2\pi)^{\frac{d}{2}} \text{Arg} \frac{\mathbb{E}\widehat{u}(t_2, \xi)}{\mathbb{E}\widehat{u}(t_1, \xi)} - \sum_{|\alpha| \text{ odd}} a_\alpha (\mathbf{i}\xi)^\alpha \mathbf{i}^{-1} (t_2 - t_1) = \frac{1}{2} \sum_{|\beta|+|\widehat{\beta}| \text{ odd}}^{p_2} \mathbf{i}^{|\beta|+|\widehat{\beta}|-1} \xi^{\beta+\widehat{\beta}} b_\beta b_{\widehat{\beta}} (t_2 - t_1).$$

We can choose the Fourier modes $\xi_k \in \mathcal{Q}_1$ with $k = 1, \dots, \widetilde{K} \geq |\mathcal{Q}_1|$. According to the assumption on \mathcal{Q}_1 , there exists a unique solution for

$$\mathbf{y}_{\text{even}} = \mathbf{A}_{\text{even}} \mathbf{c}_{\text{even}}, \mathbf{y}_{\text{odd}} = \mathbf{A}_{\text{odd}} \mathbf{c}_{\text{odd}},$$

where

$$(\mathbf{y}_{\text{even}})_k = \frac{2(2\pi)^{\frac{d}{2}}}{(t_2 - t_1)} \log \frac{\mathbb{E}\widehat{u}(t_2, \xi_k)}{\mathbb{E}\widehat{u}(t_1, \xi_k)} - \sum_{|\alpha| \text{ even}} a_\alpha (\mathbf{i}\xi_k)^\alpha, k \leq \widetilde{K},$$

$$(\mathbf{y}_{\text{odd}})_k = \frac{2(2\pi)^{\frac{d}{2}}}{(t_2 - t_1)} \log \frac{\mathbb{E}\widehat{u}(t_2, \xi_k)}{\mathbb{E}\widehat{u}(t_1, \xi_k)} - \sum_{|\alpha| \text{ even}} a_\alpha (\mathbf{i}\xi_k)^\alpha, k \leq \widetilde{K}.$$

Here $(\mathbf{A}_{\text{even}})_{k\gamma} = \xi^\gamma$ and

$$(\mathbf{c}_{\text{even}})_\gamma = \sum_{\beta+\widehat{\beta}=\gamma} \mathbf{i}^{|\beta|+|\widehat{\beta}|} b_\beta b_{\widehat{\beta}} \quad (16)$$

for even $|\gamma| \leq 2p_2$; and $(\mathbf{A}_{\text{even}})_{k\gamma} = \xi^\gamma$ and

$$(\mathbf{c}_{\text{odd}})_\gamma = \sum_{\beta+\widehat{\beta}=\gamma} \mathbf{i}^{|\beta|+|\widehat{\beta}|-1} b_\beta b_{\widehat{\beta}} \quad (17)$$

for odd $|\gamma| \leq 2p_2 - 1$. Although the vectors \mathbf{c}_{even} and \mathbf{c}_{odd} are unique, the vector b_β is uniquely determined up to an equivalent class of the solutions of (16)-(17). \square

3.2 Data space spanned by the solution trajectory of linear SPDE

We present interesting findings on the data spaces associated with three types of linear SPDEs: parabolic, hyperbolic, and Schrödinger equation. To this end, we impose more conditions on the drift and diffusion operators of SPDEs. In this subsection, we denote $H := L^2(\mathcal{D})$.

3.2.1 Parabolic SPDE

Assume that $-\mathcal{L} : H \rightarrow H$ is a linear, densely defined, closed operator and is also admissible (see Definition 2.1 of [34]), i.e.,

$$\|(z + \mathcal{L})^{-1}\|_{H \rightarrow H} \leq \frac{C}{1 + |z|}, \text{ for all } z \in \mathbb{C}/\Sigma_\delta,$$

where the constant $C > 0$ and the sector region $\Sigma_\delta \subset \mathbb{C}$ is defined by

$$\Sigma_\delta = \{z \in \mathbb{C} : |\arg(z)| \leq \delta\}, \delta \in (0, \frac{\pi}{2}).$$

Then by [42, Theorem 1], there exists an operator \mathcal{A}_L defined by $\mathcal{A}_L = \sum_{k=-L}^L c_k e^{-z_k t} (z_k + \mathcal{L})^{-1}$, $c_k, z_k \in \mathbb{C}$, such that

$$\|e^{\mathcal{L}t} - \mathcal{A}_L(t)\|_{H \rightarrow H} = \mathcal{O}(e^{-cL})$$

uniformly on the time interval $[t_0, \Lambda t_0]$ with $0 < c = \mathcal{O}(1/\log(\Lambda))$. Here $t_0 > 0$, $L \in \mathbb{N}^+$ and $\Lambda > 1$. In particular, for $t \in [t_0, T]$ that $t_0 = \epsilon^\kappa$, $\kappa > 0$, with $\epsilon \in (0, 1)$ sufficiently small, one can take $L = C_{\mathcal{L}}(\kappa)|\log(\epsilon)|^2$ such that

$$\|e^{\mathcal{L}t} - \mathcal{A}_L(t)\|_{H \rightarrow H} \lesssim \epsilon \quad (18)$$

for some constant $C_{\mathcal{L}}(\kappa) > 0$ ([34, Corollary 2.3]).

If \mathcal{L} is a strongly elliptic operator of even order p_1 , then there exists $\mu > 0$ such that $-\mathcal{L}_\mu = -\mathcal{L} + \mu$ is admissible (see e.g., [46]). Let $u_0(x) = \sum_{k=1}^{\infty} c_k \phi_k(x) \in H$ with $c_k \in \mathbb{R}$ and ϕ_k being the orthonormal basis corresponding to the dominant operator $-\mathcal{L}_\mu$. Here $(\lambda_k, \phi_k(x))_{k \geq 1}$ are eigenpairs of $-\mathcal{L}_\mu$ sorted by $\Re \lambda_k$ in ascending order include the multiplicity. It is known that by Wely's law, the growing speed satisfies $\Re \lambda_k = \mathcal{O}(k^{\frac{p_1}{d}})$. For simplicity, we also assume that \mathcal{G} is a linear closed operator of order p_2 , and commutes with \mathcal{L} . Denote the corresponding eigenvalue of \mathcal{G} by $(q_k)_{k \geq 1}$ sorted by $\Re q_k$ in ascending order including the multiplicity.

Now we present the analysis for the data space spanned by stochastic parabolic equation (7). It can be seen that the solution of (7) satisfies [16]

$$u(t, x) = e^{\mu t} \sum_{k=1}^{\infty} c_k e^{-\lambda_k t} \phi_k(x) + \sum_{k=1}^{\infty} \int_0^t e^{\mu(t-s)} e^{-\lambda_k(t-s)} q_k R_k \phi_k(x) \circ dW(s), \text{ a.s.} \quad (19)$$

Here $R(x) = \sum_{k=1}^{\infty} R_k \phi_k(x)$ and $\mathcal{G} \phi_k = q_k \phi_k$, $q_k \in \mathbb{C}$. In particular, in the multiplicative noise case, we have that

$$u(t, x) = e^{\mu t} \sum_{k=1}^{\infty} c_k e^{-\lambda_k t} e^{q_k W(t)} \phi_k(x), \text{ a.s.} \quad (20)$$

Theorem 3.3. *Let $\epsilon \in (0, 1)$. Suppose that $-\mathcal{L} + \mu$ is admissible and that u_0 is \mathcal{F}_0 -measurable satisfying $|c_k|_{L^2(\Omega; \mathbb{R})} \leq \theta k^{-\gamma}$ for some $\theta > 0, \gamma > \frac{1}{2}$.*

- (Multiplicative noise case) *Assume that $R = u$ and $\lim_{k \rightarrow \infty} \Re(\lambda_k) - 2\Re(q_k)^2 > 0$. For any $t \in [0, T]$, there exists a linear space $V \subset H$ of dimension $C_{\mathcal{L}}|\log(\epsilon)|^2$ such that*

$$\|u(t) - P_V u(t)\|_{L^2(\Omega; H)} \lesssim \epsilon(1 + \|u_0\|_{L^2(\Omega; H)}) . \quad (21)$$

- (Additive noise case) *Assume that R is a given function and $\sum_{k=1}^{\infty} \frac{|q_k|^2 |R_k|^2}{\Re(\lambda_k)^{1-\theta_1}} < \infty$ for some $\theta_1 \in (0, 1]$. For any $t \in [0, T]$, there exists a linear space $V \subset H$ of dimension $C_{\mathcal{L}}|\log(\epsilon)|^2$ such that (21) holds.*

Here P_V is the projection operator onto V .

Proof. We only show the details in deriving (21) in the multiplicative noise. Those in the additive noise are similar, and their main difference lies on dealing with the stochastic integral (see Appendix A.4 for more details).

Let $u_{\widetilde{M}}(t, x) = e^{\mu t} \sum_{k=1}^{\widetilde{M}} c_k e^{-\lambda_k t} e^{q_k W(t)} \phi_k(x)$ denote the Galerkin approximation with $\widetilde{M} \in \mathbb{N}^+$. Then we have that

$$\|u_{\widetilde{M}}(t, \cdot) - u(t, \cdot)\|_H^2 = e^{2\mu t} \sum_{k=\widetilde{M}+1}^{\infty} c_k^2 e^{-2\Re(\lambda_k)t} e^{2\Re(q_k)W(t)}.$$

Since $\lim_{k \rightarrow \infty} [\Re(\lambda_k) - 2\Re(q_k)^2] > 0$, we can find $\widetilde{K} \in \mathbb{N}^+$ such that $\mu - \Re(\lambda_k) + \Re(q_k)^2 < 0$ after $k \geq \widetilde{K}$.

This, together with the property of conditional expectation and (15), we have that for $\widetilde{M} \geq \widetilde{K}$,

$$\mathbb{E}\|u_{\widetilde{M}}(t, \cdot) - u(t, \cdot)\|_H^2 = \sum_{k=\widetilde{M}+1}^{\infty} \mathbb{E}[c_k^2] e^{2\mu t - 2\Re(\lambda_k)t + 2\Re(q_k)^2 t} \leq \theta^2 \frac{\widetilde{M}^{1-2\gamma}}{2\gamma - 1}. \quad (22)$$

Let $M_\epsilon \geq \tilde{K}, L_\epsilon > 0$ be determined later and define

$$w_\epsilon = \sum_{k=1}^{M_\epsilon} c_k \sum_{l=0}^{L_\epsilon} (-1)^l \frac{(\lambda_k t - \mu t)^l}{l!} e^{q_k W(t)} \phi_k(x).$$

Then for each t , w_ϵ sits in the linear space

$$V_1 = \text{span} \left\{ \sum_{k=1}^{M_\epsilon} c_k (-1)^l \frac{(\lambda_k t - \mu t)^l}{l!} e^{q_k W(t)} \phi_k(x), l = 0, 1, \dots, L_\epsilon \right\}.$$

By the Taylor expansion and Minkowski's inequality, as well as the independent increment property of $W(\cdot)$, we have that

$$\begin{aligned} & \|u_{M_\epsilon}(t, \cdot) - w_\epsilon(t, \cdot)\|_{L^2(\Omega; H)}^2 \\ & \leq \left\| \sum_{k=1}^{M_\epsilon} c_k \phi_k(x) e^{q_k W(t)} \sum_{l=L_\epsilon+1}^{\infty} (-1)^l \frac{(\lambda_k t - \mu t)^l}{l!} \right\|_{L^2(\Omega; H)}^2 \\ & \leq \sum_{k=1}^{M_\epsilon} \mathbb{E}[|c_k|^2] \|e^{q_k W(t)}\|_{L^2(\Omega; \mathbb{R})}^2 \left| \sum_{l=L_\epsilon+1}^{\infty} (-1)^l \frac{(\lambda_k t - \mu t)^l}{l!} \right|^2 \\ & \leq \sum_{k=1}^{M_\epsilon} \mathbb{E}[|c_k|^2] \|e^{q_k W(t)}\|_{L^2(\Omega; \mathbb{R})}^2 \frac{1}{[(L_\epsilon + 1)!]^2}. \end{aligned}$$

Here we require that $\sup_{k \leq M_\epsilon} |\lambda_k - \mu| t + \sup_{k \leq M_\epsilon} 2\Re(q_k)^2 t \leq 1$, i.e., $t \in [0, \inf_{k \leq M_\epsilon} \frac{1}{|\lambda_k - \mu| + 2\Re(q_k)^2}]$. According to (15), it follows that for $t \in [0, \inf_{k \leq M_\epsilon} \frac{1}{|\lambda_k - \mu| + 2\Re(q_k)^2}]$,

$$\begin{aligned} \|u_{M_\epsilon}(t, \cdot) - w_\epsilon(t, \cdot)\|_{L^2(\Omega; H)}^2 & \leq \sum_{k=1}^{M_\epsilon} \mathbb{E}[|c_k|^2] e^{2\Re(q_k)^2 t} \frac{1}{[(L_\epsilon + 1)!]^2} \\ & \leq \theta^2 \frac{M_\epsilon^{1-2\gamma}}{2^\gamma - 1} e^{-2L_\epsilon + 1}. \end{aligned}$$

Letting $L_\epsilon = \frac{1}{2} |\log(\epsilon)|$ and $M_\epsilon = \tilde{K} + \epsilon^{\frac{2}{1-2\gamma}}$ with $\epsilon \in (0, 1)$, and using (22), we have that

$$\begin{aligned} & \|u(t, \cdot) - w_\epsilon(t, \cdot)\|_{L^2(\Omega; H)} \\ & \leq \|u(t, \cdot) - u_{M_\epsilon}(t, \cdot)\|_{L^2(\Omega; H)} + \|u_{M_\epsilon}(t, \cdot) - w_\epsilon(t, \cdot)\|_{L^2(\Omega; H)} \lesssim \epsilon(1 + \|u_0\|_{L^2(\Omega; H)}). \end{aligned}$$

Next, we deal with the case that $t \in [\inf_{k \leq M_\epsilon} \frac{1}{|\lambda_k - \mu| + 2\Re(q_k)^2}, T]$. By (18), by taking

$$\kappa = \left| \sup_{k \leq M_\epsilon} \log(|\lambda_k - \mu| + 2\Re(q_k)^2) \right| / |\log(\epsilon)|,$$

there exists \mathcal{A}_L which is an approximation of $e^{\frac{\epsilon}{2}t}$ such that $\|e^{-\frac{\epsilon}{2}t} - \mathcal{A}_L\|_{H \rightarrow H} \lesssim \epsilon$ with $t \in [t_0, T]$ such that $t_0 = \epsilon^\kappa$, and $L = C_{\frac{\epsilon}{2}}(\kappa) |\log \epsilon|^2$. As a consequence, by using the property (15) of Brownian motion and using the fact that $\lim_{k \rightarrow \infty} [\Re(\lambda_k) - 2\Re(q_k)^2] > 0$, we have

$$\begin{aligned} & \|(e^{-\frac{\epsilon}{2}t} - \mathcal{A}_L) e^{\frac{\epsilon}{2}t + \mathcal{G}W(t)} u_0\|_{L^2(\Omega; H)}^2 \\ & \lesssim \epsilon^2 \mathbb{E} \|e^{\frac{\epsilon}{2}t + \mathcal{G}W(t)} u_0\|_H^2 \lesssim \epsilon^2 \sum_k e^{-[\Re(\lambda_k) - \mu]t} e^{2\Re(q_k)^2 t} \mathbb{E}[c_k^2] \\ & \lesssim \epsilon^2 \mathbb{E} [\|u_0\|_H^2]. \end{aligned}$$

Therefore, for $t \in [\inf_{k \leq M_\epsilon} \frac{1}{|\lambda_k - \mu| + 2\Re(q_k)^2}, T]$, there exists a linear space V_2 of dimension $L = C_{\frac{\epsilon}{2}}(\kappa) |\log \epsilon|^2$ such that

$$\|u(t, \cdot) - P_{V_2} u(t, \cdot)\|_{L^2(\Omega; H)} \lesssim \epsilon(1 + \|u_0\|_{L^2(\Omega; H)}).$$

By taking V as the linear space containing $V_1 \cup V_2$, we complete the proof for any $t \in [0, T]$. \square

Note that the assumption $\lim_{k \rightarrow \infty} \Re(\lambda_k) - 2\Re(q_k)^2 > 0$ in Theorem 3.3 is imposed for the sake of simplicity. One may replace this condition by that $\lim_{k \rightarrow \infty} c_1 \Re(\lambda_k) - \Re(q_k)^2 > 0$ with c_1 sufficiently close to 1.

3.2.2 Hyperbolic SPDE

In this part, we show the behavior of solution trajectory for hyperbolic SPDEs, which is intrinsically different from the parabolic case. Consider the following stochastic transport equation in Stratonovich sense,

$$\begin{aligned} du(t, x) + c(x) \cdot \nabla u(t, x) \circ dW(t) &= 0, \\ u(0, x) &= u_0(x), \end{aligned} \quad (23)$$

where $x \in \mathcal{D}$, $t \in [0, T]$, and $c(\cdot)$ is a vector-valued function. Its equivalent Itô's formulation reads

$$\begin{aligned} du(t, x) + c(x) \cdot \nabla u(t, x) dB(t) &= \frac{1}{2} \sum_{i=1}^d \sum_{j=1}^d c_i(x) \nabla_{x_i} (c_j(x) \nabla_{x_j} u(t, x)) dt, \\ &= \frac{1}{2} c(x) \cdot \nabla (c(x) \cdot \nabla u(t, x)) dt. \end{aligned} \quad (24)$$

Thanks to the corresponding particle formulation

$$dX(t) = -c(X(t)) \circ dW(t), X(0) = x, \quad (25)$$

the solution of (23) can be understood as follows. By the chain rule and characteristic line method, we have that

$$u(X_{0,t}(x), t) = u_0(x).$$

Here $X_{0,t}(x)$ denotes the solution of (25) starting at time 0 with initial state x and ending at time t . As a consequence, $u(y, t) = u_0(X_{t,0}(y))$ if the characteristic line does not intersect.

In this case, we can define the following two correlation functions in space and time in the average sense:

$$K(x, y) = \int_0^T \mathbb{E} [u(s, x) u(s, y)] ds, \quad G(s, t) = \int_{\mathcal{D}} \mathbb{E} [u(t, x) u(s, x)] dx,$$

where $x, y \in \mathcal{D}$, $s, t \in [0, T]$. Note that $K(\cdot, \cdot)$ and $G(\cdot, \cdot)$ are the kernels of symmetric semi-positive compact integral operators on H and $L^2([0, T])$, respectively.

Lemma 3.4. *Let $c(\cdot) \in \mathcal{C}^{p+1}(\mathcal{D})$ ($p \in \mathbb{N}$) be a velocity field and $u_0 \in \mathcal{C}^p(\mathcal{D})$. Then there exists a subspace V of dimension $o(\epsilon^{-\frac{2}{p}})$ such that*

$$\|P_V u - u\|_{L^2(\Omega; L^2([0, T]; H))} \lesssim \epsilon. \quad (26)$$

Proof. Notice that the corresponding Itô's formulation of (25) is

$$dX(t) = -c(X(t)) dW(t) - \frac{1}{2} \frac{\partial}{\partial x} c(X(t)) c(X(t)) dt.$$

Since $c(\cdot) \in \mathcal{C}^{p+1}(\mathcal{D})$ and \mathcal{D} is a compact set, by [38, Corollary 4.6.7] (see also [36, Chapter 1, section 1.1]), we have that $X_{s,t}(\cdot) \in \mathcal{C}^p(\mathcal{D})$ for any $s \leq t \in [0, T]$.

Notice that the Jacobian matrix $Y(t) = \frac{\partial X(t)}{\partial x}$ of $X(t)$ satisfies

$$Y(t) = I - \int_0^t \frac{\partial}{\partial x} c(X(t)) Y(t) \circ dW(t)$$

and that its inverse matrix $Z(t)$ satisfies that

$$Z(t) = I + \int_0^t Z(u) \frac{\partial}{\partial x} c(X(t)) \circ dW(t).$$

Thus, by the chain rule, $G(s, t) = \int_{\mathcal{D}} \mathbb{E}u(t, x)u(s, x)dx = \int_{\mathcal{D}} \mathbb{E}u(t, X_{t,0}(x))u(s, X_{s,0}(x))dx$ is differentiable with respect to x . Since $X_{s,t}(\cdot)$ is \mathcal{C}^p -differentiable, one can also show that $G(s, t)$ is \mathcal{C}^p -differentiable since $c(\cdot)$ and its derivatives up to order p are bounded thanks to the compactness of \mathcal{D} .

Notice that the eigenvalues of K and G are non-negative satisfying $\lambda_1 \geq \lambda_2 \geq \dots \geq \lambda_j \geq \dots$ with $\lambda_j \rightarrow 0$ as $j \rightarrow \infty$. The differentiability of $G(s, t)$, i.e., $G(s, t) \in \mathcal{C}^p([0, T]^2)$ leads to $\lambda_j = o(j^{-(p+1)})$ (see, e.g., [47]).

Define V_K^k and V_G^k ($k \in \mathbb{N}^+$) as the linear spaces spanned by the k leading eigenfunctions of $K(x, y)$ and $G(s, t)$, respectively. It holds that

$$\int_0^T \mathbb{E} \|u(t, \cdot) - P_{V_K^k} u(t, \cdot)\|_{L^2(\mathcal{D})}^2 dt = \int_{\mathcal{D}} \mathbb{E} \|u(\cdot, x) - P_{V_G^k} u(\cdot, x)\|_{L^2([0, T])}^2 dx = \sum_{j=k+1}^{\infty} \lambda_j.$$

This, together with $\lambda_j = o(j^{-(p+1)})$, yields that

$$\sum_{j=k+1}^{\infty} \lambda_j = o(k^{-p}),$$

which completes the proof. \square

The above analysis also indicates that a large number of parameters and data as well as an expensive training process are required to approximate a differential hyperbolic operator with rich trajectory dynamics. In contrast, the data space related to differential parabolic operator is limited to train the approximation.

3.2.3 Stochastic Schrödinger equation

For the stochastic nonlinear Schrödinger equation, we consider

$$du = \mathbf{i}\mathcal{L}u dt + \mathbf{i}\mathcal{G}u \circ dW(t). \quad (27)$$

Here the elliptic operator \mathcal{L} of even order is a linear closed symmetric operator and self-adjoint. As a consequence, the spectrum of \mathcal{L} is lying on the real axis.

Let $u_0(x) = \sum_{k=1}^{\infty} c_k \phi_k(x) \in H_{\mathbb{C}} := L^2(\mathcal{D}; \mathbb{C})$ with $c_k \in \mathbb{C}$ and $\phi_k \in H_{\mathbb{C}}$ being the orthonormal basis corresponding to the dominant operator $-\mathcal{L}$. Here $(\lambda_k, \phi_k(x))_{k \geq 1}$ are eigenpairs of $-\mathcal{L}$ sorted by λ_k in ascending order include the multiplicity. For simplicity, we also assume that the linear closed operator \mathcal{G} commutes with \mathcal{L} and has the real spectrum such that $\mathcal{G}^*\mathcal{G}$ is admissible. Denote the corresponding eigenvalue of \mathcal{G} by $(q_k)_{k \geq 1}$ include the multiplicity.

For (27), the solution satisfies

$$u(t, x) = \sum_{k=1}^{\infty} c_k e^{\mathbf{i}\lambda_k t} e^{\mathbf{i}q_k W(t)} \phi_k(x).$$

By the chain rule, one can see that its mass is preserved over time [15], i.e., $\|u(t, \cdot)\|_{H_{\mathbb{C}}} = \|u(0, \cdot)\|_{H_{\mathbb{C}}}$, a.s. Below we present an interesting finding for the data space of the stochastic Schrödinger equation in the weak topology.

Proposition 3.5. *Let $\epsilon \in (0, 1)$. Assume that the elliptic operator \mathcal{L} of even order is a linear closed symmetric and self-adjoint, and commutes with linear closed operator \mathcal{G} of real spectrum. In addition assume that $\mathcal{G}^*\mathcal{G}$ is admissible. Suppose that u_0 is \mathcal{F}_0 -measurable satisfying $|c_k|_{L^2(\Omega; \mathbb{R})} \leq \theta k^{-\gamma}$ for some $\theta > 0, \gamma > \frac{1}{2}$. Assume that $\lim_{k \rightarrow \infty} \Re(\lambda_k) - 2\Re(q_k)^2 > 0$. For any $t \in [0, T]$, there exists a linear space $V \subset H_{\mathbb{C}}$ of dimension $C_{\mathcal{L}} |\log(\epsilon)|^2$ such that*

$$\|\mathbb{E}u(t) - \mathbb{E}P_V u(t)\|_{L^2(\Omega; H_{\mathbb{C}})} \lesssim \epsilon(1 + \|u_0\|_{L^2(\Omega; H_{\mathbb{C}})}), \quad (28)$$

Here P_V is the projection operator onto V .

Proof. First, we can consider the weak approximation error of the Galerkin method, i.e., $u_{\widetilde{M}}(t, x) = \sum_{k=1}^{\widetilde{M}} c_k e^{i\lambda_k t} e^{iq_k W(t)} \phi_k(x)$ with $\widetilde{M} \in \mathbb{N}^+$.

Then by (15), the independent increment of Brownian motion and the property conditional expectation, it holds that

$$\mathbb{E}[u_{\widetilde{M}}(t, x) - u(t, x)] = \sum_{k=\widetilde{M}+1}^{\infty} \mathbb{E}[c_k] e^{i\lambda_k t} e^{-\frac{1}{2}q_k^2 t} \phi_k(x).$$

Taking H_C -norm on both sides of the above equality, we have that

$$\|\mathbb{E}[u_{\widetilde{M}}(t, \cdot) - u(t, \cdot)]\|_{H_C}^2 \leq \sum_{k=\widetilde{M}+1}^{\infty} \mathbb{E}[|c_k|^2] e^{-q_k^2 t} \leq \theta^2 \frac{\widetilde{M}^{1-2\gamma}}{2\gamma-1} \sup_{k \geq \widetilde{M}+1} e^{-q_k^2 t} \lesssim \widetilde{M}^{1-2\gamma}. \quad (29)$$

Let $M_\epsilon, L_\epsilon > 0$ be determined later and define

$$w_\epsilon = \sum_{k=1}^{M_\epsilon} c_k \sum_{l=0}^{L_\epsilon} (-1)^l \frac{(\frac{1}{2}q_k^2 t)^l}{l!} e^{i\lambda_k t} \phi_k(x).$$

For each t , w_ϵ is in the space

$$V_t = \text{span} \left\{ \sum_{k=1}^{M_\epsilon} c_k (-1)^l \frac{(\frac{1}{2}q_k^2 t)^l}{l!} e^{i\lambda_k t} \phi_k(x), l = 0, 1, \dots, L_\epsilon \right\}.$$

By the Taylor expansion and Minkowski's inequality, as well as (15), we have that for $t \leq 2 \inf_{k \leq M_\epsilon} \frac{1}{q_k^2}$,

$$\begin{aligned} & \|\mathbb{E}[u_{M_\epsilon}(t, \cdot)] - w_\epsilon(t, \cdot)\|_{L^2(\Omega; H)}^2 \\ & \leq \left\| \sum_{k=1}^{M_\epsilon} c_k \phi_k(x) e^{i\lambda_k t} \sum_{l=L_\epsilon+1}^{\infty} (-1)^l \frac{(\frac{1}{2}q_k^2 t)^l}{l!} \right\|_{L^2(\Omega; H)}^2 \\ & \leq \sum_{k=1}^{M_\epsilon} \mathbb{E}[|c_k|^2] \frac{1}{[(L_\epsilon+1)!]^2} \leq \theta^2 \frac{M_\epsilon^{1-2\gamma}}{2\gamma-1} e^{-2L_\epsilon}. \end{aligned}$$

Letting $L_\epsilon = \lceil \log(\epsilon) \rceil$ and $M_\epsilon = \epsilon^{\frac{1}{1-2\gamma}}$ with $\epsilon \in (0, 1)$, we have that

$$\|u_{M_\epsilon}(t, \cdot) - w_\epsilon(t, \cdot)\|_{L^2(\Omega; H)} \lesssim \epsilon. \quad (30)$$

For $t \in [\inf_{k \leq M_\epsilon} \frac{1}{q_k^2}, T]$, using (18) with $\kappa = \frac{\sup_{k \leq M_\epsilon} |\log(q_k^2)|}{|\log \epsilon|}$ and $L = C_{\mathcal{L}}(\kappa) |\log(\epsilon)|^2$, we have that there exists an operator \mathcal{A}_L such that

$$\|e^{i\mathcal{L}t} (e^{-\frac{1}{2}\mathcal{G}^* \mathcal{G}t} - \mathcal{A}_L(t)) u_0\|_{L^2(\Omega; H)}^2 \lesssim \epsilon^2 \|e^{i\mathcal{L}t} u_0\|_{L^2(\Omega; H)}^2 \lesssim \epsilon^2 \|u_0\|_{L^2(\Omega; H)}^2. \quad (31)$$

Here we also use the fact that $e^{i\mathcal{L}t}$ is unitary.

By combining the above estimates (29)-(31), we complete the proof. \square

It should be noticed that the strong analysis of the data space spanned by the solution trajectory depends on the initial regularity, which is similar as in the hyperbolic case. Note that the assumption that $\mathcal{G}^* \mathcal{G}$ is admissible is useful deriving (31). If it fails, then (31) may not hold due to the loss of (18).

In the additive noise case, one could obtain the similar weak convergence analysis for the data space since the expectation of the stochastic integral is 0.

4 Proposed Algorithm for Stoch-IDENT

In this section, we present our proposed algorithm for Stoch-IDENT described in Section 2.2. We mainly focus on the case where the data $U_n : \Gamma \rightarrow \mathbb{R}$ is assumed to be sampled from a strong solution $u_n := u(\omega_n) : [0, T] \times \mathcal{D} \rightarrow \mathbb{R}$ of (1) with $\mathcal{D} \subset \mathbb{R}$ and $\omega_n \in \Omega$ for $n = 1, \dots, N$. The extension to multi-dimensional spaces or stochastic systems is straightforward.

4.1 Drift and diffusion feature systems

Consider the Itô integral form of (1) evaluated at a sequence of equidistant time points $0 = t_0 < t_1 < t_2 < \dots < t_I = T$ as follows

$$u(t_i, x) - u(t_{i-1}, x) = \sum_{k=1}^K a_k \int_{t_{i-1}}^{t_i} F_k(t, x) dt + \sum_{j=1}^J b_j \int_{t_{i-1}}^{t_i} G_j(t, x) dW_t, \quad i = 1, \dots, I, \quad \forall x \in \mathcal{D}. \quad (32)$$

Applying the left Riemann sum and Euler-Maruyama scheme to approximate the integral and stochastic integral respectively in (32) formally gives

$$u(t_i, x) - u(t_{i-1}, x) = \sum_{k=1}^K a_k F_k(t_{i-1}, x) \Delta t + \sum_{j=1}^J b_j G_j(t_{i-1}, x) (W(t_i) - W(t_{i-1})) + \mathcal{O}((\Delta t)^{3/2}), \quad (33)$$

where $\Delta t = t_i - t_{i-1}$ for each i . Take expectation on (33) and we get

$$\mathbb{E}[u(t_i, x)] - \mathbb{E}[u(t_{i-1}, x)] = \Delta t \sum_{k=1}^K a_k \mathbb{E}[F_k(t_{i-1}, x)] + \mathcal{O}((\Delta t)^{3/2}) \quad (34)$$

For a set of points $\{x_m\}_{m=1}^M \subset \mathcal{D}$, we define the *drift feature matrix* as

$$\mathbf{F} := \Delta t \cdot \begin{pmatrix} \mathbb{E}[F_1(t_1, x_1)] & \mathbb{E}[F_2(t_1, x_1)] & \cdots & \mathbb{E}[F_K(t_1, x_1)] \\ \mathbb{E}[F_1(t_1, x_2)] & \mathbb{E}[F_2(t_1, x_2)] & \cdots & \mathbb{E}[F_K(t_1, x_2)] \\ \vdots & \vdots & \ddots & \vdots \\ \mathbb{E}[F_1(t_I, x_M)] & \mathbb{E}[F_2(t_I, x_M)] & \cdots & \mathbb{E}[F_K(t_I, x_M)] \end{pmatrix} \in \mathbb{R}^{IM \times K}, \quad (35)$$

where each column is obtained by flattening expected values of candidate drift features evaluated at discrete time-space points. We define the *drift response vector* as

$$\mathbf{y} := \begin{pmatrix} \mathbb{E}[u(t_1, x_1)] - \mathbb{E}[u(t_0, x_1)] \\ \mathbb{E}[u(t_1, x_2)] - \mathbb{E}[u(t_0, x_2)] \\ \vdots \\ \mathbb{E}[u(t_I, x_M)] - \mathbb{E}[u(t_I, x_M)] \end{pmatrix} \in \mathbb{R}^{IM}. \quad (36)$$

The relation (34) can thus be compactly expressed as

$$\mathbf{y} = \mathbf{F}\mathbf{a} + \mathcal{O}((\Delta t)^{3/2}), \quad (37)$$

where $\mathbf{a}^\top = (a_1, \dots, a_K) \in \mathbb{R}^K$ is the unknown feature coefficient vector.

According to (4), the expectation of the squared drift residual

$$r^2(t_i, x, \mathbf{a}) := \left(u(t_i, x) - u(t_{i-1}, x) - \Delta t \sum_{k=1}^K a_k F_k(t_{i-1}, x) \right)^2, \quad (38)$$

should be close to

$$\mathbb{E} \left(\sum_{j=1}^J b_j G_j(t_{i-1}, x) (W(t_i) - W(t_{i-1})) \right)^2 = \Delta t \sum_{j=1}^J \sum_{s=1}^J b_j b_s \mathbb{E} [G_j(t_{i-1}, x) \cdot G_s(t_{i-1}, x)], \quad (39)$$

for any $i = 1, \dots, I$ and $x \in \mathcal{D}$, and we define the i -th *diffuse feature matrix* as

$$\mathbf{G}_i := \Delta t \cdot \begin{pmatrix} \mathbb{E} \left[\int_{\mathcal{D}} G_1(t_{i-1}, y) \cdot G_1(t_{i-1}, y) dy \right] & \cdots & \mathbb{E} \left[\int_{\mathcal{D}} G_1(t_{i-1}, y) \cdot G_J(t_{i-1}, y) dy \right] \\ \vdots & \ddots & \vdots \\ \mathbb{E} \left[\int_{\mathcal{D}} G_J(t_{i-1}, y) \cdot G_1(t_{i-1}, y) dy \right] & \cdots & \mathbb{E} \left[\int_{\mathcal{D}} G_J(t_{i-1}, y) \cdot G_J(t_{i-1}, y) dy \right] \end{pmatrix} \in \mathbb{R}^{J \times J}, \quad (40)$$

where $\oint_{\mathcal{D}} g(y) dy := |\mathcal{D}|^{-1} \cdot \int_{\mathcal{D}} g(y) dy$ denotes the average integral and $|\mathcal{D}|$ is the Lebesgue measure of the interval \mathcal{D} . Moreover, we define the i -th *diffuse response* as

$$\zeta_i(\mathbf{a}) = \mathbb{E} \left[\oint_{\mathcal{D}} r^2(t_i, y, \mathbf{a}) dy \right] \in \mathbb{R}, i = 1, \dots, I. \quad (41)$$

We emphasize that only discrete observations of sampled strong solutions are available, thus the aforementioned feature matrices and responses are generally not accessible. We describe the necessary approximations of the feature systems in Section 5. We call the drift feature matrix together with the drift feature response as a *drift feature system*; and the diffusion feature matrices with the diffusion responses as a *diffusion feature system*.

Remark 4.1. *Extending the feature systems to adapt for identifying SDEs with multi-dimensional space or stochastic systems such as stochastic Schrödinger equations is straightforward. For multi-dimensional space, the candidate drift and diffusion features will be augmented with partial derivatives involving all spatial variables; and for systems, products of features associated with individual system variables will be included. Moreover, the average integrals in the diffusion system will be replaced by average integrals with respect to the space domain.*

4.2 Subspace Pursuit (SP) for candidate drift models

Instead of directly searching for the optimal drift model, we propose to produce a sequence of candidate models consisting of different active features. More precisely, we consider the problem

$$\begin{aligned} \min_{\mathbf{c} \in \mathbb{R}^K} \|\mathbf{F}\mathbf{c} - \mathbf{y}\|_2^2 \\ \text{s.t. } \|\mathbf{c}\|_0 = k \end{aligned} \quad (42)$$

for $k = 1, 2, \dots, K$, where $\|\mathbf{c}\|_0 := |\text{supp}(\mathbf{c})|$ counts the number of non-zero entries of a vector \mathbf{c} . A solution of (42) yields a candidate drift model with exactly k active features. This strategy of sequentially generating candidate models was initiated in [33] for identifying constant coefficient PDEs. It converts a challenging combinatorial problem of feature selection to a sequence of minimization problems and efficiently avoids redundant or missing candidates resulted from continuous regularization [48, 10, 37]. Although (42) is NP-hard [45], a greedy algorithm, Subspace Pursuit (SP) [18], was found to be particularly effective [33, 54] in finding sparse coefficients whose supports cover the true supports. We adopt the same algorithm in this work for generating candidate drift models and include the pseudo-code of SP in Algorithm 2 in Appendix C for completeness.

4.3 New Quadratic Subspace Pursuit (QSP) for candidate diffusion models

Suppose that we have obtained an estimated drift coefficient vector $\hat{\mathbf{a}} \in \mathbb{R}^K$. To identify the diffusion features, we propose to consider the following sparse regression problem with quadratic measurements

$$\begin{aligned} \min_{\mathbf{c} \in \mathbb{R}^J} \sum_{i=1}^I (\mathbf{c}^\top \mathbf{G}_i \mathbf{c} - \zeta_i(\hat{\mathbf{a}}))^2 \\ \text{s.t. } \|\mathbf{c}\|_0 = j \end{aligned} \quad (43)$$

for $j = 1, 2, \dots, J$. Similarly to the strategy for the drift part, we generate a sequence of candidate diffusion models from (43). We note that (43) is a sparse regression problem with quadratic measurements, which is related to the problem of phase retrieval [3, 2, 24, 12]. Most of the existing methods deal with sparsity-inducing through ℓ_1 -regularization. In this work, we propose a new algorithm, Quadratic Subspace Pursuit (QSP) that finds a j -sparse vector in a greedy manner. Algorithm 1 shows the pseudo-code. The proposed QSP searches for a j -sparse vector mainly by iterating two operations stated in Algorithm 1 (**Step 1**) *Expanding*: include unselected variables that have the strongest potential in reducing the regression residuals; and (**Step 2**) *Shrinking*: discard selected variables associated with regression coefficients of small magnitudes.

More specifically, we define $\eta_i^{(0)} = \zeta_i$ for $i = 1, \dots, I$ and set $\mathcal{I}^0 = \emptyset$. In the ℓ -th iteration of **Step 1**, we take the strategy of coordinate descent and examine the squared sum of the regression errors resulted from using individual variables:

$$q_s^{(\ell+1)} = \min_c \sum_{i=1}^I (\mathbf{G}_i^{s,s} c - \eta_i^{(\ell)})^2. \quad (44)$$

Here $\mathbf{G}_i^{s,s}$ is the s -th diagonal element of the i -th diffusion feature matrix; $\eta_i^{(\ell)}$ is the quadratic regression error associated with the i -th measurement (**Step 4**) using the current candidate variables; and s is any index of variables not selected in the previous iteration. Then we include the variables with the smallest j errors, yielding a set of candidate indices $\tilde{\mathcal{I}}^{\ell+1}$ with size at most $2j$.

In the ℓ -th iteration of **Step 2**, we solve the regression problem with quadratic measurements

$$\bar{\mathbf{c}}^{(\ell+1)} \in \arg \min_{\substack{\mathbf{c} \in \mathbb{R}^J \\ [\mathbf{c}]_{(\tilde{\mathcal{I}}^{\ell+1})^c} = \mathbf{0}}} \sum_{i=1}^I (\mathbf{c}^\top \mathbf{G}_i \mathbf{c} - \zeta_i(\hat{\mathbf{a}}))^2 \quad (45)$$

only using the selected variables indexed by $\tilde{\mathcal{I}}^{\ell+1}$. Then we keep the indices of the entries of $\bar{\mathbf{c}}^{(\ell+1)}$ with the j largest absolute values to be the set $\mathcal{I}^{\ell+1}$. In **Step 3**, we update the regression coefficients using the updated set of variables. The algorithm terminates when the regression error does not improve.

The proposed QSP is a greedy algorithm and can be regarded as an extension of SP to the problem of sparse regression with quadratic measurements. In particular, **Step 1** of QSP generalizes the SP's projection of residuals to the feature column space (**Step 1** in Algorithm 2) to coordinate regression with respect to the residuals. And **Step 2** of QSP replaces the SP's linear regression (**Step 2** in Algorithm 2) with a nonlinear regression problem. Since (45) does not have closed-form solutions, QSP can be more computationally expensive than SP. However, we empirically find that QSP converges within 5-10 iterations, and it is effective at finding the support of the true diffusion coefficients. We report its performance in Section 6 and leave the algorithmic analysis to the future works.

4.4 Model selection via time integration

Given any set of the drift coefficient vectors $\{\mathbf{a}_1, \mathbf{a}_2, \dots, \mathbf{a}_M\} \subset \mathbb{R}^K$, we propose to evaluate

$$S_{\text{drift}}(\mathbf{a}_m) := I^{-1} \cdot \sum_{i=1}^I \int_{\mathcal{D}} \left(\sum_{k=1}^K a_{m,k} \int_0^{t_i} \mathbb{E}[F_k(s, x)] ds + \mathbb{E}[u(0, x)] - \mathbb{E}[u(t_i, x)] \right)^2 dx \quad (46)$$

for $m = 1, \dots, M$, where $a_{m,k}$ denotes the k -th entry of \mathbf{a}_m . We set $\hat{\mathbf{a}} := \arg \min_{m=1, \dots, M} S_{\text{drift}}(\mathbf{a}_m)$. Given an estimation $\hat{\mathbf{a}}$ for the drift coefficients and any set of diffusion coefficient vectors $\{\mathbf{b}_1, \dots, \mathbf{b}_L\} \subset \mathbb{R}^J$, we define

$$S_{\text{diffuse}}(\mathbf{b}_l | \hat{\mathbf{a}}) := I^{-1} \cdot \sum_{i=1}^I \int_{\mathcal{D}} \left(\mathbb{E}[R_i^2(x, \hat{\mathbf{a}})] - \mathbb{E} \int_0^{t_i} \left(\sum_{j=1}^J b_{l,j} G_j(s, x) \right)^2 ds \right)^2 dx \quad (47)$$

for $l = 1, \dots, L$, where $R_i^2(x, \hat{\mathbf{a}}) := \left(\sum_{k=1}^K \hat{a}_k \int_0^{t_i} F_k(s, x) ds + u(0, x) - u(t_i, x) \right)^2$ and $b_{l,j}$ is the j -th entry of \mathbf{b}_l . Notice that (47) quantifies the integral form of (4) for a pair of candidate diffusion and drift coefficients. Similarly to the choice of drift coefficients, we set the optimal $\hat{\mathbf{b}} := \arg \min_{l=1, \dots, L} S_{\text{diffuse}}(\mathbf{b}_l | \hat{\mathbf{a}})$ as the optimal diffusion coefficient vector associated with a drift coefficient vector $\hat{\mathbf{a}}$. Consequently, the SPDE associated with these optimal coefficient vectors as expressed in (5) is the identified model.

The following result shows that if the estimated drift coefficients are close to the true drift coefficients, then the corresponding value of (46) is low.

Lemma 4.2. *Suppose $\mathbf{a}^* = (a_1^*, \dots, a_K^*)$ is the true drift coefficient vector of the underlying SPDE. Assume that $\sup_{(t,x) \in [0,T] \times \mathcal{D}} |\mathbb{E}[F_k(t, x)]| < \infty$ for $k = 1, \dots, K$. Then there exist some constants $C > 0$ such that for any $\mathbf{a} \in \mathbb{R}^K$*

$$S_{\text{drift}}(\mathbf{a}) \leq C \|\mathbf{a}^* - \mathbf{a}\|_2^2.$$

Algorithm 1: Proposed Quadratic Subspace Pursuit (QSP)

Input: Diffuse feature system $\mathbf{G}_i \in \mathbb{R}^{J \times J}$ (40), $\zeta_i \in \mathbb{R}$ (41), for $i = 1, \dots, I$, and $j \in \{1, \dots, J\}$.

Initialization: $\ell = 0$;
Set $\eta_i^{(0)} = \zeta_i$ for $i = 1, \dots, I$;
Set $\mathcal{I}^0 = \emptyset$.

while *True* **do**

Step 1. Compute $q_s^{(\ell+1)} = \min_c \sum_{i=1}^I (\mathbf{G}_i^{s,s} c - \eta_i^{(\ell)})^2$ for $s \notin \mathcal{I}^\ell$
Set $\tilde{\mathcal{I}}^{\ell+1} = \mathcal{I}^\ell \cup \{ \text{indices corresponding to the } j \text{ smallest } |q_s^{(\ell+1)}| \}$;

Step 2. Compute $\bar{\mathbf{c}}^{(\ell+1)} \in \arg \min_{\substack{\mathbf{c} \in \mathbb{R}^J \\ [\mathbf{c}]_{(\tilde{\mathcal{I}}^{\ell+1})^c} = \mathbf{0}}} \sum_{i=1}^I (\mathbf{c}^\top \mathbf{G}_i \mathbf{c} - \zeta_i)^2$
Set $\mathcal{I}^{\ell+1} = \{ \text{Indices of the entries of } \bar{\mathbf{c}}^{(\ell+1)} \text{ with the } j \text{ largest absolute values} \}$;

Step 3. Compute $\hat{\mathbf{c}}^{(\ell+1)} \in \arg \min_{\substack{\mathbf{c} \in \mathbb{R}^J \\ [\mathbf{c}]_{(\mathcal{I}^{\ell+1})^c} = \mathbf{0}}} \sum_{i=1}^I (\mathbf{c}^\top \mathbf{G}_i \mathbf{c} - \zeta_i)^2$

Step 4. Compute $\eta_i^{(\ell+1)} = [\hat{\mathbf{c}}^{(\ell+1)}]_{\mathcal{I}^{\ell+1}}^\top [\mathbf{G}_i]_{\mathcal{I}^{\ell+1}} [\hat{\mathbf{c}}^{(\ell+1)}]_{\mathcal{I}^{\ell+1}} - \zeta_i$ for $i = 1, 2, \dots, I$;
if $\sum_{i=1}^I (\eta_i^{(\ell+1)})^2 > \sum_{i=1}^I (\eta_i^{(\ell)})^2$ **then**
| Set $\mathcal{I}^* = \mathcal{I}^\ell$ and $\hat{\mathbf{c}}^* = \hat{\mathbf{c}}^{(\ell)}$, then break;
end
else
| Set $\ell \leftarrow \ell + 1$ and continue;
end

end

Output: Indices of chosen features \mathcal{I}^* with $|\mathcal{I}^*| = j$ and reconstructed coefficients $\hat{\mathbf{c}}^* \in \mathbb{R}^J$ with $\text{supp}(\hat{\mathbf{c}}^*) = \mathcal{I}^*$.

See Appendix B.1 for the proof. Moreover, we find that if both drift and diffusion coefficients are accurately estimated, then (47) will be bounded as follows.

Lemma 4.3. Suppose $\mathbf{a}^* = (a_1^*, \dots, a_K^*)$ and $\mathbf{b}^* = (b_1^*, \dots, b_J^*)$ are the true drift and diffusion coefficient vectors of the underlying SPDE, respectively. Assume that $\sup_{(t,x) \in [0,T] \times \mathcal{D}} \mathbb{E}[|F_k(t,x)|^2] < +\infty$ and $\sup_{(t,x) \in [0,T] \times \mathcal{D}} \mathbb{E}[|G_j(t,x)|^2] < +\infty$ for every $k = 1, \dots, K$ and $j = 1, \dots, J$. Then there exist some constants $C > 0$ such that for any $\mathbf{a} \in \mathbb{R}^K$ and $\mathbf{b} \in \mathbb{R}^J$, the following inequality

$$S_{\text{diffuse}}(\mathbf{b}|\mathbf{a}) \leq C[(\|\mathbf{a}\| + \|\mathbf{a}^*\|)^2(\|\mathbf{a} - \mathbf{a}^*\|^2) + (\|\mathbf{b}\| + \|\mathbf{b}^*\|)^2\|\mathbf{b} - \mathbf{b}^*\|^2] \quad (48)$$

holds.

See Appendix B.2 for the proof. Hence, by comparing the values of (47) associated with different candidates of diffusion coefficients estimation, the smallest one indicates the optimal choice.

4.5 Problem reformulation by sample average approximation

As the mean values in the feature systems introduced in Section 4.1 are not available, we approximate them by their respective sample averages. In particular, we consider the following estimators

$$\mathbb{E}[F_k(t,x)] \approx \frac{1}{N} \sum_{n=1}^N F_k^n(t,x), \text{ and } \mathbb{E}[u(t,x)] \approx \frac{1}{N} \sum_{n=1}^N U_n(t,x) \quad (49)$$

for $k = 1, \dots, K$ and any $(t,x) \in [0,T] \times \mathcal{D}$, where $F_k^n(t,x) := F_k(t,x,\omega_n)$ for $\omega_n \in \Omega$; and we define \mathbf{F}^N and \mathbf{y}^N as the N sample mean approximations of \mathbf{F} (35) and \mathbf{y} (36) respectively by replacing their entries with the corresponding estimators (49). The expectations in the diffusion feature matrix (40) and the diffusion responses (41) are similarly approximated by sample averages. Explicitly, denoting

$G_j^n(t, x) := G_j(t, x, \omega_n)$, we approximate

$$\mathbb{E} \left[\int_{\mathcal{D}} G_s(t_i, y) \cdot G_j(t_i, y) dy \right] \approx \frac{1}{N} \sum_{n=1}^N \int_{\mathcal{D}} G_s^n(t_i, y) \cdot G_j^n(t_i, y) dy, \quad (50)$$

for any $s, j \in \{1, \dots, J\}$ in (40) and denote \mathbf{G}_i^N as the resulting matrix for $i = 1, \dots, I$. Given an estimated drift coefficient vector $\hat{\mathbf{a}} = (\hat{a}_1, \dots, \hat{a}_K)$, we also approximate

$$\zeta_i \approx \zeta_i^N(\hat{\mathbf{a}}) := \frac{1}{N} \sum_{n=1}^N \int_{\mathcal{D}} (r_i^n(y, \hat{\mathbf{a}}))^2 dy \quad (51)$$

where

$$r_i^n(x, \hat{\mathbf{a}}) := U_n(t_i, x) - U_n(t_{i-1}, x) - \Delta t \sum_{k=1}^K \hat{a}_k F_k^n(t_{i-1}, x) \quad (52)$$

and $\Delta t > 0$ is the interval size of the grid in the time dimension. Consequently, we obtain a surrogate of (42) as follows

$$\begin{aligned} \min_{\mathbf{c} \in \mathbb{R}^K} & \|\mathbf{F}^N \mathbf{c} - \mathbf{y}^N\|_2^2 \\ \text{s.t. } & \|\mathbf{c}\|_0 = k \end{aligned} \quad (53)$$

for $k = 1, \dots, K$. Suppose $\hat{\mathbf{a}}^N$ is an estimated diffusion coefficient vector, then we consider the following surrogate of (43)

$$\begin{aligned} \min_{\mathbf{c} \in \mathbb{R}^J} & \sum_{i=1}^I (\mathbf{c}^\top \mathbf{G}_i^N \mathbf{c} - \zeta_i^N(\hat{\mathbf{a}}^N))^2 \\ \text{s.t. } & \|\mathbf{c}\|_0 = j \end{aligned} \quad (54)$$

for $j = 1, \dots, J$. As the feature systems are approximated via sample means, the identified drift and diffusion coefficients are random variables.

The following result shows that as the number of sample paths $N \rightarrow \infty$, any convergent sequence of minimizers of the sample average approximation (53) converges to a minimizer of (42) almost surely.

Theorem 4.4. Denote $f_O(\mathbf{c}) := \|\mathbf{F}\mathbf{c} - \mathbf{y}\|_2^2$ and $f_N(\mathbf{c}) := \|\mathbf{F}^N \mathbf{c} - \mathbf{y}^N\|_2^2$. Assume that $\mathbf{c}^* \in \mathbb{R}^K$ with $\|\mathbf{c}^*\|_0 = k$ is a local minimizer of (42), i.e., there exists some $\varepsilon > 0$ such that $f_O(\mathbf{c}^*) \leq f_O(\mathbf{c})$ for any \mathbf{c} with $\|\mathbf{c} - \mathbf{c}^*\|_2 < \varepsilon$. Then the problem (53) converges to (42) almost surely in the following sense:

1. The optimal value of (42) converges almost surely to the optimal value of (53).
2. Define $\Psi_N := \arg \min_{\mathbf{c} \in \mathbb{R}^K} \{f_N(\mathbf{c}) : \|\mathbf{c}\|_0 = k\}$ and $\Psi_O := \arg \min_{\mathbf{c} \in \mathbb{R}^K} \{f_O(\mathbf{c}) : \|\mathbf{c}\|_0 = k\}$, then

$$\limsup_{N \rightarrow \infty} \Psi_N \subset \Psi_O \text{ a.s.} \quad (55)$$

where \limsup is understood in the Kuratowski-Mosco sense [49]:

$$\limsup_{N \rightarrow \infty} X_N := \{x \in \mathbb{R}^K : \exists (x_{N_k})_{k=1}^\infty \text{ with } \lim_{k \rightarrow \infty} x_{N_k} = x \text{ and } x_{N_k} \in X_{N_k}, \forall k \in \mathbb{N}\}.$$

Proof. This theorem follows from a series of results in [58]. From the Strong Law of Large Numbers (SLLN), $f_N(\mathbf{c})$ converges to $f_O(\mathbf{c})$ almost surely for any $\mathbf{c} \in \mathbb{R}^K$. Since \mathbf{c}^* is a local minimizer of f_O , by Theorem 5.1 of [58], f_N is lower semi-continuously convergent almost surely to f_O on the set $C_k := \{\mathbf{c} : \|\mathbf{c}\|_0 = k\}$ (See Definition 2.6 [58]). Hence, the conditions in Theorem 4.1 of [58] are satisfied, which implies the conclusions. \square

Following [58], the analogous results with convergence in probability also hold. Based on the almost surely convergent subsequence of minimizers specified in (55), the asymptotic behavior of the surrogate (54) can be similarly deduced.

Theorem 4.5. For any $\mathbf{a} \in \mathbb{R}^K$ and $\mathbf{c} \in \mathbb{R}^J$, denote $g_O(\mathbf{c}, \mathbf{a}) := \sum_{i=1}^I (\mathbf{c}^\top \mathbf{G}_i \mathbf{c} - \zeta_i(\mathbf{a}))^2$ and $g_N(\mathbf{c}, \mathbf{a}) := \sum_{i=1}^I (\mathbf{c}^\top \mathbf{G}_i^N \mathbf{c} - \zeta_i^N(\mathbf{a}))^2$. Assume that for any $\mathbf{a} \in \mathbb{R}^K$, $\mathbf{c}^* \in \mathbb{R}^J$ with $\|\mathbf{c}^*\|_0 = j$ is a local minimizer of (43), i.e., there exists some $\varepsilon > 0$ such that $g_O(\mathbf{c}^*, \mathbf{a}) \leq g_O(\mathbf{c}, \mathbf{a})$ for any \mathbf{c} with $\|\mathbf{c} - \mathbf{c}^*\|_2 < \varepsilon$. Then the problem (54) converges to (43) almost surely in the following sense.

1. For any $\hat{\mathbf{a}} \in \limsup_{N \rightarrow \infty} \Psi_N$ as defined in (55); that is, there exists a subsequence $(\hat{\mathbf{a}}_{N_k})_{k=1}^\infty$ with $\hat{\mathbf{a}}_{N_k} \in \Psi_{N_k}$ that converges to $\hat{\mathbf{a}}$ almost surely, we have

$$\lim_{k \rightarrow \infty} \Phi_{N_k}(\hat{\mathbf{a}}_{N_k}) = \Phi_O(\hat{\mathbf{a}}) \text{ a.s.}$$

where $\Phi_{N_k}(\hat{\mathbf{a}}_{N_k}) := \inf_{\mathbf{c} \in \mathbb{R}^J} \{g_{N_k}(\mathbf{c}, \hat{\mathbf{a}}_{N_k}) : \|\mathbf{c}\|_0 = j\}$ and $\Phi_O(\hat{\mathbf{a}}) := \inf_{\mathbf{c} \in \mathbb{R}^J} \{g_O(\mathbf{c}, \hat{\mathbf{a}}) : \|\mathbf{c}\|_0 = j\}$

2. Define $\Pi_N(\mathbf{a}) := \arg \min_{\mathbf{c} \in \mathbb{R}^J} \{g_N(\mathbf{c}, \mathbf{a}) : \|\mathbf{c}\|_0 = j\}$ and $\Pi_O(\mathbf{a}) := \arg \min_{\mathbf{c} \in \mathbb{R}^J} \{g_O(\mathbf{c}, \mathbf{a}) : \|\mathbf{c}\|_0 = j\}$, then for any $\hat{\mathbf{a}} \in \limsup_{N \rightarrow \infty} \Psi_N$ and the associated convergent subsequence $(\hat{\mathbf{a}}_{N_k})_{k=1}^\infty$ with $\hat{\mathbf{a}}_{N_k} \in \Psi_{N_k}$, we have

$$\limsup_{k \rightarrow \infty} \Pi_{N_k}(\hat{\mathbf{a}}_{N_k}) \subset \Pi_O(\hat{\mathbf{a}}) \text{ a.s.}$$

in the same sense of (55).

Remark 4.6. The condition that there exists a k -sparse solution to (42) which is also a local minimizer can be guaranteed by sufficient conditions involving Spark [21] or Restricted Isometry Property (RIP) [11] of \mathbf{F} ; see [5] also. In practice, certifying these properties are NP-hard [4], and empirical studies in [33] show that RIP generally does not hold for feature matrices associated with PDEs. However, the fact that \mathbf{F} is associated with derivatives of expectation values of some strong solution to a SPDE makes this assumption more feasible. At least for linear SPDEs, if the solution presents enough variation, then the drift part can be uniquely determined, see section 3.1. The condition for the j -sparse solution to (43) is similar. For more general SPDEs, we will study them in future works.

5 Implementation Details

In this section, we provide more details about implementing our Stoch-IDENT algorithm proposed in Section 4. The identification procedure for the drift part is essentially the same as introduced in [33]. In particular, when the feature operators involve spatial derivatives of u , we approximate them using 7-point Fornberg's finite differences [26]; then we multiply the estimated derivatives to approximate the nonlinear features. When running SP (Algorithm 2) for the drift candidate generation (Section 4.2), the drift feature matrix is column normalized for robust support reconstruction [33]. After obtaining the candidate drift models, we apply the trimming technique [54]. In the following, we focus on presenting important details related to identifying the diffusion features.

5.1 Details for diffusion candidate generation

For the proposed generation method for candidate diffusion models, we note that the following normalization of the quadratic measurement matrices, i.e., the diffusion feature matrices, is crucial. In particular, we introduce

$$\overline{\mathbf{G}}_i := \mathbf{\Lambda}^{-1} \mathbf{G}_i \mathbf{\Lambda}^{-1}$$

for $i = 1, \dots, I$, where $\mathbf{\Lambda} \in \mathbb{R}^{J \times J}$ is a diagonal matrix whose j -th diagonal element is the square root of the average of the j -th diagonal elements of $\{\mathbf{G}_i\}_{i=1}^I$, i.e., $\sqrt{J^{-1} \cdot \sum_{i=1}^I \mathbf{G}_i^{j,j}}$, for $j = 1, \dots, J$. When running QSP (Algorithm 1), we substitute \mathbf{G}_i with $\overline{\mathbf{G}}_i$ defined above; and after obtaining $\hat{\mathbf{b}}$, the coefficient estimate associated with $\{\mathbf{G}_i\}_{i=1}^I$ is $\hat{\mathbf{b}} \mathbf{\Lambda}^{-1}$.

For addressing the nonlinear regression problem (45), we tested with nonlinear conjugate gradient (CG) descent using various CG updating parameters [29], and find that the one proposed by Hager and Zhang [28] performs the best in our experiments.

Moreover, we propose a trimming technique to help eliminate excessive diffusion terms. Suppose $\hat{\mathbf{b}} = (\hat{b}_1, \dots, \hat{b}_J)$ is a candidate diffusion coefficient vector and $\mathcal{S}(\hat{\mathbf{b}}) = \{j = 1, \dots, J : \hat{b}_j \neq 0\}$ denotes its support. Define the score

$$\theta_j(\hat{\mathbf{b}}) := \frac{|\hat{b}_j|}{\max_{\ell \in \mathcal{S}(\hat{\mathbf{b}})} |\hat{b}_\ell|}, \text{ for } j \in \mathcal{S}.$$

The entries of $\hat{\mathbf{b}}$ with indices in $\{j \in \mathcal{S} : \theta_j(\hat{\mathbf{b}}) < \tau\}$ for some threshold $\tau > 0$ are set to zero, and its other non-zero coefficients will be estimated via the nonlinear regression. Similarly to [54], we find that this technique is effective at eliminating wrong features.

5.2 Statistical tests for detecting additive noise

We note that it requires more computational resources to identify the diffusion features: construction of the drift feature matrices and responses, solving the nonlinear regression via CG iterations, and model validation. However, these computations can all be avoided for stochastic equations with additive noise, and we propose the following strategy to garnish this efficiency.

Suppose $\hat{\mathbf{a}} = (\hat{a}_1, \dots, \hat{a}_K)$ is the estimated drift coefficient vector. We define the space average drift residuals

$$\rho_i^n(\hat{\mathbf{a}}) := \oint_{\mathcal{D}} \left(U_n(t_i, x) - U_n(t_{i-1}, x) - \Delta t \sum_{k=1}^K \hat{a}_k F_k^n(t_{i-1}, x) \right) dx$$

for $i = 1, \dots, I$ and $n = 1, \dots, N$. If the underlying SPDE has only additive noise σdW for some $\sigma \in \mathbb{R}$ and $\hat{\mathbf{a}}$ is close to the true drift coefficient vector, then the empirical distribution of $\mathcal{R}^n := \{\rho_i^n(\hat{\mathbf{a}}), i = 1, \dots, I\}$ should be approximately Gaussian with mean 0 and variance $\sigma^2 \Delta t$ for each n . We propose to apply the D'Agostino-Pearson test [17] to decide if \mathcal{R}^n deviates from a Gaussian distribution; it computes the sample kurtosis and skewness then conducts a hypothesis test on their nonlinear transformation. After conducting the tests for individual paths, we obtain N p -values $\{p_1, \dots, p_N\}$, each of which indicates the likelihood of observing \mathcal{R}^n under the null hypothesis of Gaussian distribution. To keep the false positive rate under control, we employ the Stouffer's method [52] and define

$$Z_N = N^{-1/2} \sum_{n=1}^N \Phi^{-1}(p_n),$$

which is a standard normal variable with cumulative distribution function (CDF) Φ under the null hypothesis. Then for some significance level $p^* \in (0, 1)$, we decide that the diffusion part contains multiplicative noise if $2|Z_N| \geq \Phi^{-1}(p^*)$, and it is only additive if $2|Z_N| < \Phi^{-1}(p^*)/2$. In the case multiplicative noise is detected, we will follow the diffusion identification procedure described in Section 4. When the noise is detected to be additive, we estimate σ by sample standard deviation $\hat{\sigma}$, and the identified model is simply

$$du = \sum_{k=1}^K \hat{a}_k \mathcal{F}_k(u) + \hat{\sigma} dW(t).$$

In this way, we skip the construction of the diffusion feature system and the subsequent identification procedure.

6 Numerical Experiments

In this section, we conduct numerical experiments to validate the proposed Stoch-IDENT by testing it on various SPDEs under different scenarios. In all examples, we simulate the observed trajectories by numerically solving the SPDEs via the Euler-Maruyama scheme for time discretization and appropriate schemes for the spatial variables to be explained individually. For all examples, we consider the Cauchy problems with periodic boundary conditions.

In this work, we consider **dictionaries of type (\mathbf{p}, \mathbf{q})** for integers $p \geq 0$ and $q \geq 1$, which means that we include features with spatial derivatives up to order p and multiplications of up to q terms. These dictionary parameters can be different for the dictionaries for the drift and diffusion parts.

To estimate the spatial differential features from data, we apply the classical 7-point finite difference scheme [26] with periodic boundary condition. For identifying the drift part, we adopt the trimming technique introduced in [54] to eliminate excessive features in each candidate generated from the SP (Section 4.2); the threshold parameter is fixed at 0.3. For identifying the diffusion part, the maximal number of iterations of the nonlinear CG for address (45) is set to be 1000; the initial guesses for the non-zero entries are fixed at 10; and the iteration terminates if the gradient of the loss function has a magnitude smaller than 1×10^{-14} . The maximal number of iterations for the QSP (Algorithm 1) is set to be 100, although in practice, we observe that it converges around $10 \sim 15$ iterations. The trimming threshold τ for the candidate diffusion features (Section 5.1) is also fixed at 0.3.

For performance evaluation for both drift and diffusion parts, we compare the support of the estimated coefficient vector $\mathbf{c} = (c_1, \dots, c_K)$ with the support of the ground truth coefficient vector $\mathbf{c}^* = (c_1^*, \dots, c_K^*)$ using:

- Precision

$$\text{Prec} := \frac{\text{TP}}{\text{TP} + \text{FP}}$$

- Accuracy

$$\text{ACC} := \frac{\text{TP} + \text{TN}}{\text{TP} + \text{FP} + \text{TN} + \text{FN}}$$

- Recall

$$\text{Recall} := \frac{\text{TP}}{\text{TP} + \text{FN}}$$

- F1-score

$$F_1 := 2 \cdot \frac{\text{Prec} \times \text{Recall}}{\text{Prec} + \text{Recall}}$$

where TP, TN, FP, and FN are true positive, true negative, false positive, and false negative, respectively. These metrics all bounded between 0 and 1 with 1 being the best. In addition, we evaluate the coefficient errors using the following metrics:

- Relative in-coefficient error

$$E_{\text{in}}(\mathbf{c}, \mathbf{c}^*) = \frac{\sqrt{\sum_{i \in \text{supp}(\mathbf{c}^*)} (c_i - c_i^*)^2}}{\|\mathbf{c}^*\|_2} \times 100\% \quad (56)$$

- Relative out-coefficient error

$$E_{\text{out}}(\mathbf{c}, \mathbf{c}^*) = \frac{\sqrt{\sum_{i \notin \text{supp}(\mathbf{c}^*)} c_i^2}}{\|\mathbf{c}\|_2} \times 100\% \quad (57)$$

The relative in-coefficient error measures the deviation of the estimated coefficients for the true features, while the relative out-coefficient error measures the magnitude of the coefficients for the wrongly identified features.

6.1 General performances of Stoch-IDENT

In this section, we test Stoch-IDENT on N independent trajectories generated from various typical SPDEs. In particular, we consider identifying:

Stochastic transport equation with multiplicative noise (see e.g. [25]):

$$du = (3u_x + 0.5u_{xx})dt + u_x dW(t), \quad \text{for } x \in [-\pi, \pi) \text{ and } t \in (0, 0.1) \quad (58)$$

with the initial condition $u(0, x) = 0.1 \exp(\sin(4x - 0.2)) \cdot \cos(5x + 0.8)$.

Stochastic Korteweg-de Vries (KdV) equation with additive noise (see e.g. [19]):

$$du = (-6uu_x - u_{xxx})dt + 7dW(t), \quad \text{for } x \in [-\pi, \pi) \text{ and } t \in (0, 0.05) \quad (59)$$

with the initial condition $u(0, x) = \exp(\sin(3x - 0.2)) \cdot \cos(2x + 0.8) + 4.0$.

Stochastic Burgers equation with both additive and multiplicative noise (see e.g. [7]):

$$du = (3uu_x + 0.5u_{xx})dt + (5 + 2u)dW(t), \quad \text{for } x \in [-\pi, \pi) \text{ and } t \in (0, 0.05) \quad (60)$$

with the initial condition $u(0, x) = 3 \sin^2(x - 1) + 2 \cos(2x) + 5 \sin(5x + 2.0) + 1.0$.

For all the SPDEs above, we employ periodic boundary conditions, and the solution datasets are collected on a uniform grid with 300 points in time and 100 points in space. To ensure stability, the grids are up-sampled in time by 50 times when generating the data through numerical evolution. We use dictionaries of type (4, 3) for the drift part, and type (2, 2) for the diffusion part. For each choice

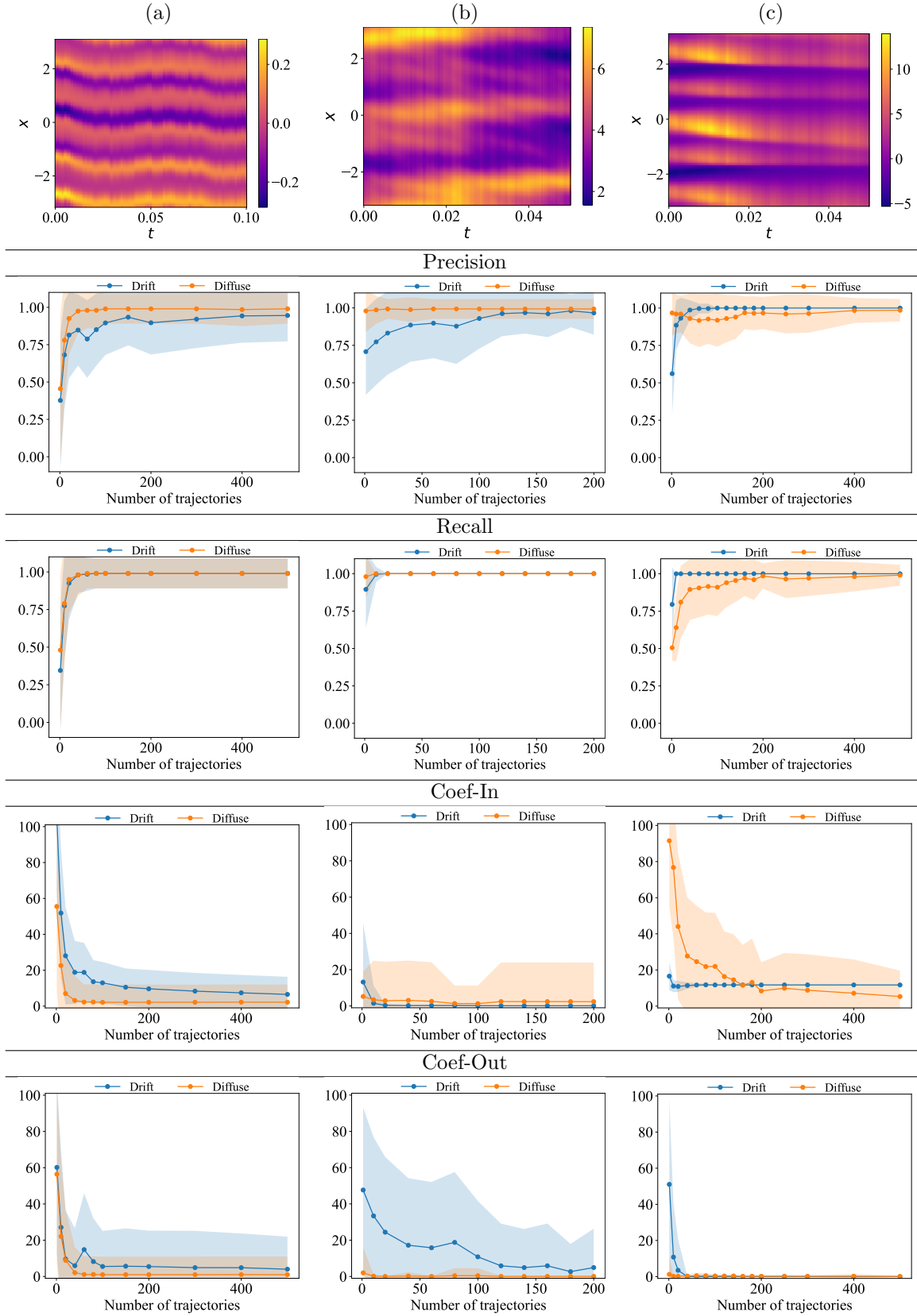


Figure 1: Identification performance versus the number of trajectories. Column (a) Stochastic transport equation (58) (b) Stochastic KdV equation (59) (c) Stochastic Burgers equation (60). As the number of observed trajectories increases, we evaluate the identification results by precision, recall, relative in-coefficient errors, and relative out-coefficient errors. For each setup, we sample 100 independent paths.

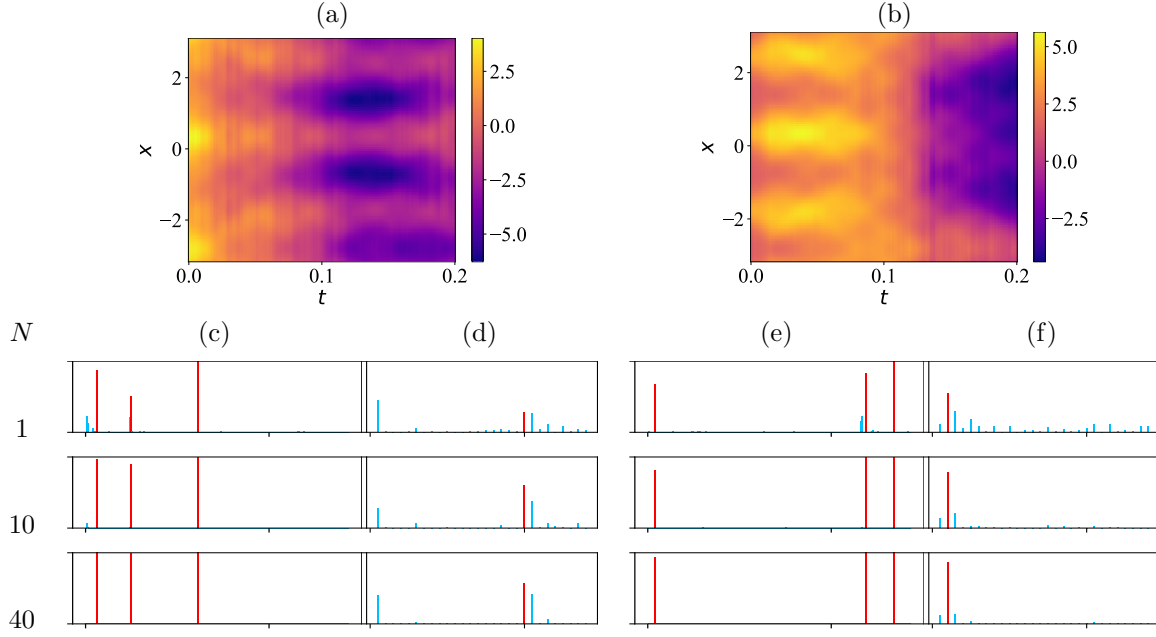


Figure 2: Identification of the stochastic NLS equation (61). For a sample path ρ , we show (a) $u := \text{Re}(\rho)$ and (b) $v := \text{Im}(\rho)$. With $N = 1, 10$, and 40 trajectories, we show the frequency of identified features for (c) the drift part of u ; (d) the diffusion part of u ; (e) the drift part of v ; and (f) the diffusion part of v in 100 independent experiments. For (c)-(f), the y axes range from 0 to 1; the x axes are the indices of candidate features; the red and blue bars correspond to the true and wrong features, respectively.

of sample size N , we run Stoch-IDENT for 100 independent experiments and examine the statistics of the evaluation metrics. In Figure 1, we present the identification results as follows: the first row displays sample trajectories; the second row shows the relationship between N and precision; the third row reports recall; the fourth row presents the relative in-coefficient error; and the last row illustrates the relative out-coefficient error. We make the following observations: **(1)** For all tested SPDEs, we observe that as the number of trajectories N increases, the identification accuracy (measured by precision and recall) improves, while the coefficient estimation error decreases. **(2)** A mixture of additive and multiplicative noise makes identifying the diffusion part more challenging. Specifically, the diffusion part is easiest to identify in purely additive noise (e.g., the KdV equation), harder in purely multiplicative noise (e.g., the transport equation), and most difficult in a mixture of both (e.g., the Burgers equation). Notably, as N increases, the identified diffusion parts in the Burgers example often consist of only additive noise. This occurs because when identifying the drift part via (42), the lack of fit is measured using the squared ℓ_2 -norm. Consequently, the model assumption for the drift residual (52) treats it as a homoscedastic random normal vector with independent components, which can also be interpreted as a diffusion part with additive noise. Thus, if the underlying SPDE contains additive noise, our proposed detection method (Section 5.2) can effectively identify it. However, if the multiplicative noise is strong—causing the drift residual to deviate significantly from a normal distribution—the diffusion part is more likely to be correctly identified. That said, as noise strength increases, more sample paths are required to approximate the means accurately via sample averages and recover the covariance structure.

6.2 Identification of complex SPDE

To demonstrate the versatility of the proposed Stoch-IDENT, we test it to identify the following well-known complex SPDE – **stochastic nonlinear Schrödinger (NLS)** with multiplicative noise (see e.g. [14, 13]):

$$d\rho = 5i\rho_{xx}dt + i|\rho|^2\rho dt + i\rho dW(t), \quad \text{for } x \in [-\pi, \pi) \text{ and } t \in (0, 0.2) \quad (61)$$

Table 1: The most frequently identified model from 100 independent experiments of identifying the stochastic nonlinear Schrödinger equation (61) using varying numbers of trajectories. For each identified feature, we also report the mean value of the associated coefficients \pm the standard deviation. The setup of the experiments is the same as that reported in Figure 2.

No. of traj.	Most frequently identified model
1	$\begin{cases} du &= (9.760_{\pm 0.559}u + 4.435_{\pm 0.061}u_{xx} + 0.888_{\pm 0.024}u^3) dt + 2.832_{\pm 0.027}dW(t) \\ dv &= (-1.012_{\pm 0.041}u^2v - 4.772_{\pm 0.082}v_{xx} - 0.950_{\pm 0.040}v^3) dt + 0.987_{\pm 0.003}udW(t) \end{cases}$
10	$\begin{cases} du &= (4.942_{\pm 0.092}u_{xx} + 0.994_{\pm 0.068}u^3 + 1.002_{\pm 0.101}uv^2) dt + 1.000_{\pm 0.014}vdW(t) \\ dv &= (-1.004_{\pm 0.103}u^2v - 4.960_{\pm 0.010}v_{xx} - 1.009_{\pm 0.084}v^3) dt + 1.001_{\pm 0.018}udW(t) \end{cases}$
40	$\begin{cases} du &= (4.935_{\pm 0.049}u_{xx} + 0.989_{\pm 0.037}u^3 + 0.995_{\pm 0.054}uv^2) dt + 0.998_{\pm 0.010}vdW(t) \\ dv &= (-1.010_{\pm 0.059}u^2v - 4.950_{\pm 0.048}v_{xx} - 0.997_{\pm 0.040}v^3) dt + 1.004_{\pm 0.009}udW(t) \end{cases}$
Reference model	
	$\begin{cases} du &= (5u_{xx} + u^3 + uv^2) dt \pm vdW(t) \\ dv &= (-u^2v - 5v_{xx} - v^3) dt \pm udW(t) \end{cases}$

where $\rho = u + \mathbf{i}v$ is a complex-valued function; and $W(t)$ is a real-valued Wiener process. The initial condition is $u(0, x) = \exp(\sin(2x + 1)) + 1$ and $v(0, x) = \exp(\cos(3x + 1)) + 1$. The setup for the grid and dictionaries are identical with the previous experiments. In Figure 2 (a) and (b), we show the real and imaginary part of a sample path. For the number of sample paths $N = 1, 10$ and 40 , we conduct 100 independent experiments and report the frequency of the identified features in (c)-(f), where red bars correspond to the correct features, and the blue bars correspond to the wrong ones. We have the following observations: **(1)** For both drift and diffusion parts, correct features are more frequently detected and the wrong ones are less frequently found as N increases. **(2)** Correct drift features are more easily identified compared to the diffusion ones. We see that for both real and imaginary parts, most wrong drift features are never identified, and the correct drift features immediately dominate even when there is only a single path available. In contrast, for the real diffusion part, we see that many wrong features are frequently identified when N is small, and they persist even when $N = 40$ although their frequency drops and the dominating feature eventually corresponds to the correct one. **(3)** Identification is not symmetric. Unlike the SPDE (61) itself, the identification performances for the real and imaginary parts are not symmetric. We see that the identification for the imaginary diffusion part is much more efficient than that for the real diffusion part; even when $N = 1$, the most frequently identified imaginary diffusion feature is the correct one. Whereas it requires multiple paths for the real diffusion part.

In Table 1, we report the most frequently identified models when $N = 1, 10$ and 40 . For the coefficients, we show the sample means and standard deviations of the estimated values. We observe that **(1)** Although the correct features can be frequently identified (see Figure 2 (c) and (e)), a single path ($N = 1$) is insufficient to yield the correct model. **(2)** In this NLS example, a few more sample paths ($N = 10$) are enough to frequently identify the correct model, and the variability of the estimated coefficients is reduced when more paths are available. **(3)** In the original model (61), the imaginary diffusion part is symbolically $-udW(t)$, which is equivalent to $udW(t)$ in the sense discussed in section 3.1. Since we use positive values for the nonzero entries of the initial guesses for the nonlinear CG iterations, the estimations tend to converge to the equivalent counterparts with positive values. From (45), this sign difference is also indistinguishable; thus the coefficient errors should be measured in absolute values in this case.

6.3 Simulations from the identified model

We demonstrate the applicability of Stoch-IDENT by comparing the observed trajectory with the simulation from the identified model. For this experiment, we consider the **stochastic Allen-Cahn**

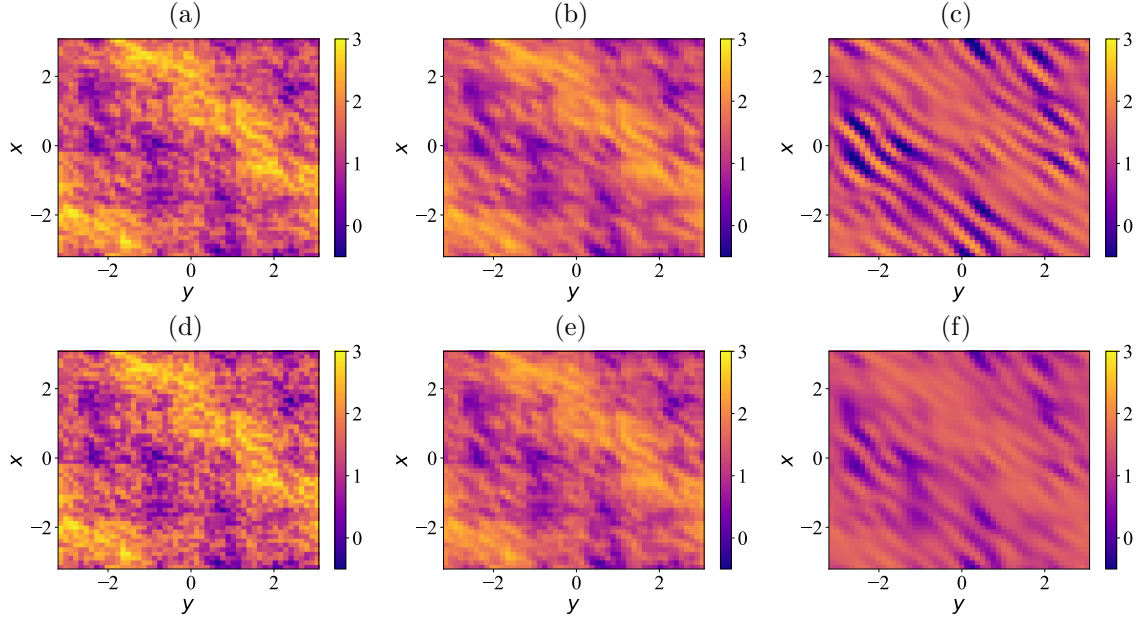


Figure 3: Comparison between a solution path of stochastic Allen-Cahn (62) at (a) $t = 8 \times 10^{-3}$ (b) $t = 2 \times 10^{-2}$, and (c) $t = 8 \times 10^{-2}$ with the simulation by the identified SPDE (63) at (d)-(f) the same time points. The identification is based on 20 trajectories sampled on a coarse grid, and the simulated dynamics exhibit a similar pattern formation to that of the true model.

equation with multiplicative noise (see e.g. [9, 1]):

$$du = (0.5\Delta u - 2(u^3 - u)) dt + (u_x + u_y)dW(t), \quad \text{for } x \in [-\pi, \pi] \text{ and } t \in (0, 0.08) \quad (62)$$

with the initial condition $u(0, x, y) = \sqrt{(\sin^2(2x) + \cos^2(2y))} + 0.5 \exp(\sin(x + y)) + \zeta(x, y)$ where $\zeta(x, y)$ is a fixed random field independently sampled from a uniform distribution $\mathcal{U}(-1, 1)$. The uniform grid for the data contains 100 points in time and 50 points in both dimensions of the space. When solving (62), we up-sample the time by 50 times. The first row of Figure 3 shows snapshots of a sample path at $t = 8 \times 10^{-3}$, $t = 2 \times 10^{-2}$, and $t = 8 \times 10^{-2}$, where stripe patterns are formed. For this example, we use dictionaries of type (3, 3) for the drift part, and type (2, 2) for the diffusion part.

With $N = 20$ trajectories, we can identify the following model

$$du = (0.333u_{xx} + 0.337u_{yy} - 2.059u^3 + 2.084u) dt + (0.726u_x + 0.850u_y) dW(t), \quad (63)$$

which contains the correct terms as in (62). The coefficients for the Laplacian and diffusion terms show lower accuracy compared to the reaction terms. This stems from numerical errors in approximating differential features when using coarse grids. However, as seen in the second row of Figure 3, when we simulate the path using the same Wiener process that drove the original dynamics, we observe similar pattern formation, ultimately producing the characteristic stripes. In practical applications, the underlying Wiener process is typically unknown. Consequently, implementing evaluation metrics like the evolution-based TEE [37] would demand computationally intensive sampling procedures [43].

6.4 Identification with random initialization

We investigate the performance of Stoch-IDENT when the observed sample paths are generated by a single SPDE with different initial conditions. For this example, we consider the **stochastic Kardar-Parisi-Zhang (KPZ) equation** with additive noise (see e.g. [30]):

$$du = (3u_{xx} + 3(u_x)^2) dt + dW(t), \quad \text{for } x \in [-\pi, \pi] \text{ and } t \in (0, 0.5) \quad (64)$$

with N initial condition $u_N(0, x) = \exp(\sin(2x) + \zeta_N(x))$ where $\zeta_N(x) \sim \mathcal{U}(-0.5, 0.5)$ are independent. The solution datasets are collected on a uniform grid with 200 points in time and 100 points in space.

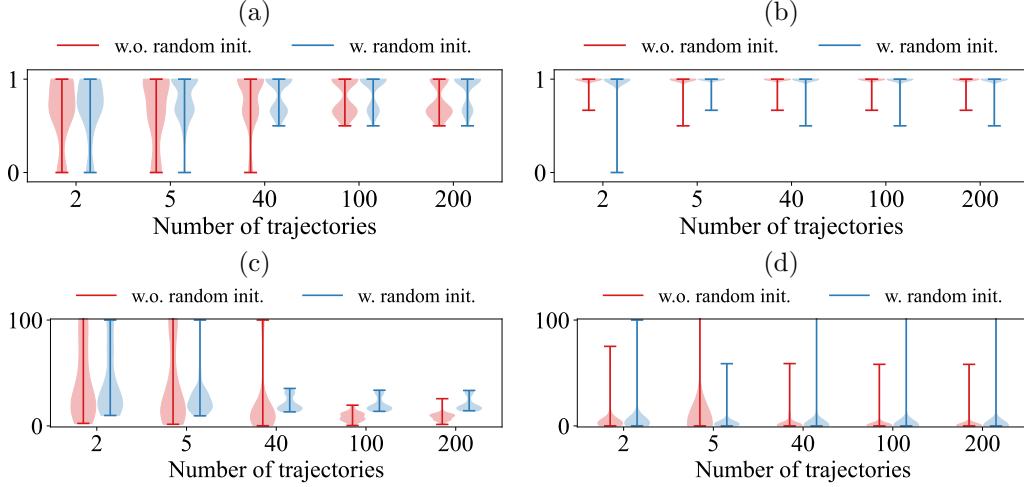


Figure 4: Comparison between identification using trajectories with or without random initializations. The underlying SPDE is the KPZ equation (64). Using violin diagrams, (a) and (b) show the F1 score of the identification accuracy for the drift and diffusion part, respectively; and (c) and (d) show the relative in-coefficient errors for the drift and diffusion part, respectively. For each setup, the result is summarized from 100 independent experiments.

As in the previous examples, the data are generated by numerically solving Equation (64), with the time grid points upsampled by a factor of 50. We adopt a dictionary of type (4, 3) for the drift term and (2, 2) for the diffusion term.

In Figure 4, we report the statistics of identification accuracy, measured by the F1 score in (a) and (b), and relative coefficient errors in (c) and (d), based on 100 independent experiments for each N (ranging from 2 to 200). For each scenario, we also present the identification results obtained using fixed initial conditions—specifically, for each path, the initial condition is generated by a fixed $\zeta(x) \sim \mathcal{U}(-0.5, 0.5)$. From the results, we observe the following: **(1)** Diversity in initial conditions improves drift identification for limited sample paths. For the diffusion term, however, we do not observe a significant benefit from using random initial conditions. In fact, in the case of additive noise, the identification accuracy for the diffusion term remains consistently high across all experiments. **(2)** Random initial conditions lead to less accurate coefficient estimation compared to fixed initial conditions. Notably, as the number of sample paths increases, the coefficient estimation errors for fixed initial conditions become lower than those for random initial conditions.

This experiment demonstrates that while using paths with different initial conditions does not hinder feature identification, a more accurate coefficient estimation in some applications may require repeated observations under the same initial conditions.

6.5 Comparison study

We compare Stoch-IDENT with e-SINDy and the Variational Bayesian (VB) method from [43], highlighting key differences. First, e-SINDy and VB find the square of the diffusion term. This forces the use of higher-order terms for simple features (e.g., $u_x dW(t)$ requires u_x^2), requires a dictionary up to $M(M+1)/2$ terms for identifying M features, and dampens small coefficients, making them hard to detect. Second, their dictionary was limited to terms like $u^q \partial_x^p u$ with integers p and q , and their experiments mainly focused on additive noise.

Numerically, we test Stoch-IDENT, e-SINDy and VB on identifying the following stochastic heat equations with multiplicative noise:

$$du = u_{xx}dt + 0.3u_x dW(t), \quad \text{for } x \in [-\pi, \pi) \text{ and } t \in (0, 0.1) \quad (65)$$

and

$$du = u_{xx}dt + (2u + 0.5u_x) dW(t), \quad \text{for } x \in [-\pi, \pi) \text{ and } t \in (0, 0.1) \quad (66)$$

both with the initial condition $u(0, x) = 0.2 \exp(\sin(3x - 0.2)) \cdot \cos(4x + 0.8)$. The setup for the grid is identical with that described in Section 6.1. We consider $N = 50$ trajectories and use a type (4, 3)

Table 2: We compare Stoch-IDENT with e-SINDy and VB [43] on stochastic heat equations with multiplicative noise: (I) $0.3u_x dW(t)$ and (II) $(2u + 0.5u_x)dW(t)$. Stoch-IDENT achieves robust identification and accurate coefficient estimation. Importantly, while e-SINDy and VB identify the squared diffusion term, Stoch-IDENT recovers the original diffusion term directly (up to equivalence).

(I) Equation (65)								
Method	Prec (\uparrow)		Recall (\uparrow)		E_{in} (\downarrow)		E_{out} (\downarrow)	
	Drift	Diffusion	Drift	Diffusion	Drift	Diffusion	Drift	Diffusion
Proposed	0.9358	0.9883	1.0	1.0	1.9201	2.7905	5.1695	0.4881
e-SINDy	0.3155	0.0	1.0	0.0	1.123	100.0	88.404	100.0
VB	0.8933	0.0	1.0	0.0	1.076	100.0	14.655	100.0
Most frequently identified model								
Proposed	$du = 0.982_{\pm 0.007}u_{xx} dt + 0.298_{\pm 0.004}u_x dW(t)$							
e-SINDy	$du = (0.989_{\pm 0.008}u_{xx} - 0.338_{\pm 0.092}u^2u_{xx} - 2.715_{\pm 1.729}u^2u_x - 5.482_{\pm 1.268}u^3) dt + \sqrt{-0.221_{\pm 0.001}u^3} dW(t)$							
VB	$du = 0.993_{\pm 0.008}u_{xx} dt + \sqrt{0.020_{\pm 0.001}} dW(t)$							
(II) Equation (66)								
Method	Prec (\uparrow)		Recall (\uparrow)		E_{in} (\downarrow)		E_{out} (\downarrow)	
	Drift	Diffusion	Drift	Diffusion	Drift	Diffusion	Drift	Diffusion
Proposed	0.8749	0.9100	1.0	0.9050	2.9829	18.4966	12.6144	9.2869
e-SINDy	0.1458	0.8175	1.0	1.0	2.190	41.313	98.518	2.4481
VB	0.7231	0.9975	1.0	1.0	3.107	41.700	35.308	0.003
Most frequently identified model								
Proposed	$du = 0.996_{\pm 0.033}u_{xx} dt + (2.029_{\pm 0.087}u + 0.415_{\pm 0.034}u_x) dW(t)$							
e-SINDy	$du = (0.986_{\pm 0.015}u_{xx} + 0.435_{\pm 0.152}u + 0.239_{\pm 0.745}uu_x^2 + (4 \text{ terms})) dt + \sqrt{0.259_{\pm 0.009}u_x^2 + 1.850_{\pm 0.051}uu_x + 3.190_{\pm 0.053}u^2 - 0.113_{\pm 0.003}u^3} dW(t)$							
VB	$du = 1.005_{\pm 0.032}u_{xx} dt + \sqrt{0.2515_{\pm 0.009}u_x^2 + 1.8248_{\pm 0.0469}uu_x + 3.1035_{\pm 0.060}u^2} dW(t)$							

Table 3: Average runtime (in seconds) of 10 runs of Stoch-IDENT when (I) the number of input trajectories is N , the dictionary for drift is of type $(4, 3)$, and the dictionary for diffusion is of type $(2, 2)$; (II) the dictionary for drift is of type $(p_{\text{drift}}, 2)$, dictionary for diffusion is of type $(2, 2)$, and $N = 20$; (III) the dictionary for diffusion is of type $(p_{\text{diffusion}}, 2)$, dictionary for drift is of type $(3, 3)$, and $N = 10$. The underlying SPDE is fixed as the stochastic transport equation (58).

(I)			(II)			(III)		
N	Time (sec.)		p_{drift}	Time (sec.)		$p_{\text{diffusion}}$	Time (sec.)	
	Drift	Diffusion		Drift	Diffusion		Drift	Diffusion
1	2.32	11.31	2	2.51	13.29	2	4.27	12.98
10	4.04	12.23	3	2.97	13.37	3	4.23	20.96
100	14.33	21.54	4	3.48	13.38	4	4.25	21.93
200	26.10	28.24	5	4.10	13.41	5	4.26	21.25
400	48.11	44.34	6	4.73	13.37	6	4.27	26.62

dictionary for both the drift and diffusion, resulting in 56 candidate features for each. For Stoch-IDENT, we keep all hyperparameters fixed as in previous experiments. For e-SINDy and VB, we use regularization parameters of 0.5 and 0.2 for drift and diffusion identification, respectively. We evaluate Stoch-IDENT, e-SINDy, and VB over 100 independent experiments and report their performance in Table 2.

For identifying (65), we observe that Stoch-IDENT achieves the highest accuracy in terms of precision and recall for both drift and diffusion, while e-SINDy and VB both fail to correctly identify the underlying diffusion feature. In reconstructing the coefficient of the true drift feature (i.e., u_{xx}), VB attains the lowest error; however, the coefficients it estimates for incorrectly identified drift features have larger magnitudes compared to those of Stoch-IDENT. We also report the most frequently identified models along with the mean and standard deviation of the reconstructed coefficients, which show that Stoch-IDENT yields the best overall identification.

For identifying (66), Stoch-IDENT continues to perform satisfactorily, while VB achieves the highest identification accuracy for the diffusion part. In this example, e-SINDy attains the lowest error in estimating the coefficient of the true drift feature, and VB yields the smallest magnitudes for the coefficients of incorrectly identified diffusion terms. Stoch-IDENT, however, demonstrates more robust performance overall. We note that this slight underperformance by Stoch-IDENT was expected, as it stems from the inherent difficulty of the sparse nonlinear regression problem in (43). In contrast, both e-SINDy and VB recover the squared diffusion term via sparse linear regression, which is more tractable. Nevertheless, based on the most frequently identified models reported in Table 2 (II), Stoch-IDENT correctly identifies the exact form of the underlying SPDE with relatively low coefficient estimation errors. e-SINDy tends to select excessive terms, and although VB identifies all correct features, it is not straightforward to infer the true form of the diffusion term from its coefficients. It is practically unlikely that the estimated coefficients would align with the required binomial coefficients. Thus, we conclude that Stoch-IDENT is effective at recovering the exact forms (up to equivalence classes) of SPDEs from data.

6.6 Time complexity of Stoch-IDENT

We study the time complexity of Stoch-IDENT¹. The runtime of our method is primarily governed by three factors: the number of input trajectories (N), the size of the dictionary for the drift terms, and the size of the dictionary for the diffusion terms.

In Table 3, we report the average runtime over 10 runs of Stoch-IDENT for identifying the stochastic transport equation (58) as these factors are varied. (I) With the dictionaries for the drift and diffusion features fixed to types $(4, 3)$ and $(2, 2)$ respectively, we vary N from 1 to 400. We observe that the time required to identify both the drift and diffusion parts grows linearly with N . The time for the diffusion

¹In this work, the data generation and identification algorithms are implemented in C++ and the construction of feature systems are realized in parallel with OpenMP. All the experiments are conducted in MacBook Pro with Apple M3 Max chip (16 threads) and 128 GB memory. The reported times include both constructions of the feature systems and the identification processes.

part is greater than that for the drift part by approximately a constant factor. (II) With $N = 10$ fixed, we increase the maximum order of partial derivatives in the dictionary for drift features. We see that this only affects the identification time of the drift part, and this relationship is linear. (III) When we increase the maximum order of partial derivatives in the dictionary for diffusion features, the identification time for the diffusion part increases linearly.

7 Conclusion

In this paper, we introduce Stoch-IDENT, a novel framework for identifying SPDEs driven by time-dependent Wiener processes with both additive and multiplicative noise structures. We provide an in-depth mathematical analysis of the identifiability of such SPDEs from data. Algorithmically, we generalize Robust-IDENT [33] to recover drift terms and design a new greedy algorithm, QSP, to identify diffusion terms. Notably, QSP is applicable to general sparse regression problems with quadratic measurements, such as phase retrieval and distance-based localization [24]. Convergence and general applications will be studied in a different work. Through a series of experiments on linear and nonlinear high-order SPDEs, we verify Stoch-IDENT's effectiveness and illustrate its behaviors. Theoretically, we prove that the Fourier modes of the initial data are essential for ensuring the uniqueness of the identified SPDEs. Furthermore, by analyzing the solution trajectory's dimension, we demonstrate the intrinsic difficulty of identifying parabolic equations compared to hyperbolic ones in general settings. This work provides a theoretical foundation for SPDE identification, generalizing identifiability analysis for deterministic PDEs [34]. While we focus on time-dependent Wiener processes here, we will generalize the algorithm and theory to space-time Wiener processes in future work.

A Some proofs in Section 3

A.1 Proof of Proposition 3.1 in additive noise case

Proof. In the additive noise case, taking the expectation directly on (9), and making use of the martingale property of the stochastic integral, we obtain that

$$\mathbb{E}\hat{u}(t_2, \xi) = \mathbb{E}\hat{u}(t_1, \xi) \exp \left((2\pi)^{-\frac{d}{2}} \sum_{|\alpha|=0}^{p_1} a_\alpha(\mathbf{i}\xi)^\alpha (t_2 - t_1) \right).$$

This implies that

$$\frac{\mathbb{E}\hat{u}(t_2, \xi)}{\mathbb{E}\hat{u}(t_1, \xi)} = \exp \left((2\pi)^{-\frac{d}{2}} \sum_{|\alpha| \text{ even}}^{p_1} a_\alpha(\mathbf{i}\xi)^\alpha (t_2 - t_1) \right) \exp \left((2\pi)^{-\frac{d}{2}} \sum_{|\alpha| \text{ odd}}^{p_1} a_\alpha(\mathbf{i}\xi)^\alpha (t_2 - t_1) \right).$$

By considering the angle and phase variables in complex domain, it follows that

$$\frac{(2\pi)^{\frac{d}{2}}}{t_2 - t_1} \log \left(\frac{\mathbb{E}\hat{u}(t_2, \xi)}{\mathbb{E}\hat{u}(t_1, \xi)} \right) = \sum_{|\alpha| \text{ even}}^{p_1} \mathbf{i}^{|\alpha|} \xi^\alpha a_\alpha, \quad (67)$$

$$\frac{(2\pi)^{\frac{d}{2}}}{t_2 - t_1} \text{Arg} \left(\frac{\mathbb{E}\hat{u}(t_2, \xi)}{\mathbb{E}\hat{u}(t_1, \xi)} \right) = \sum_{|\alpha| \text{ odd}}^{p_1} \mathbf{i}^{|\alpha|-1} \xi^\alpha a_\alpha. \quad (68)$$

Thus, we conclude that the drift coefficients is identifiable if and only if (67) and (68) admit a unique solution $a_\alpha, |\alpha| \leq p_1$. In particular, if $|t_2 - t_1| > 0$ is small, then the phase ambiguity (up to $2k\pi$ for any $k \in \mathbb{N}^+$) in (68) is removed. Hence, the standard polynomial regression argument as in the proof of [34, Theorem 3.2] leads to the unique identification result of a_α . \square

It can be seen that, to obtain unique identification of drift terms in the additive noise, it suffices to let $\mathcal{Q} = \{\xi \in \mathbb{Z}^d : \mathbb{E}\hat{u}_0(\xi) \neq 0\}$ satisfy the condition in Proposition 3.1, and assume that two time points of the averaged solutions $\mathbb{E}u(t_1, \cdot), \mathbb{E}u(t_2, \cdot)$ are given.

A.2 Diffusion identification based on pathwise information

In the additive noise case, suppose that the information of the stochastic convolution

$$\chi(t_1, t_2, \xi, W) := \int_{t_1}^{t_2} \exp\left((2\pi)^{-\frac{d}{2}} \sum_{|\alpha|=0}^n a_\alpha(\mathbf{i}\xi)^\alpha(t_2 - s)\right) \widehat{R}(\xi) dW(s), \text{ a.s.}$$

is known. According to the mild formulation (9), we show that enough Fourier modes can also guarantee the identification of the diffusion part almost surely.

Proposition A.1. *Let $\mathcal{Q}_1 = \{\xi \in \mathbb{Z}^d | \widehat{R}(\xi) \neq 0\}$ satisfy*

$$|\mathcal{Q}_1| \geq \binom{p_2 + d}{d}$$

and that \mathcal{Q}_1 is not located on an algebraic polynomial hypersurface of degree $\leq p_2$. Given $a_\alpha, |\alpha| \leq p_1$, and $\chi(t_1, t_2, \xi, W), \xi \in \mathcal{Q}_1$ for some $t_2 - t_1 > 0$, the parameters $b_\beta, |\beta| \leq p_2$, are uniquely determined by the solution at two instants $u(t_2, \cdot), u(t_1, \cdot)$.

Proof. Since $|\mathcal{Q}_1| \geq \binom{p_2 + d}{d}$, by Itô's formula, there exists Fourier modes $\xi_k, k = 1, \dots, \tilde{K}$ with $\tilde{K} \geq |\mathcal{Q}_1|$ such that $\chi(t_1, t_2, \xi_k, W)$ is Gaussian with mean 0 and covariance

$$\mathbb{E}[|\chi(t_1, t_2, \xi_k, W)|^2] = \int_{t_1}^{t_2} \sum_j \exp\left(2(2\pi)^{-\frac{d}{2}} \sum_{|\alpha| \text{ even}}^{p_1} a_\alpha(\mathbf{i}\xi)^\alpha(t_2 - s)\right) |\widehat{R}(\xi_k)|^2 ds > 0.$$

This implies that the stochastic convolution $\chi(t_1, t_2, \xi, W) \neq 0, \text{ a.s.}$ Thus, we have that

$$\begin{aligned} \chi^{-1}(t_1, t_2, \xi, W) & \left[\widehat{u}(t_2, \xi) - \widehat{u}(t_1, \xi) \exp\left((2\pi)^{-\frac{d}{2}} \sum_{|\alpha|=0}^{p_1} a_\alpha(\mathbf{i}\xi)^\alpha(t_2 - t_1)\right) \right] \\ & = \sum_{|\beta|=0}^{p_2} b_\beta(\mathbf{i}\xi)^\beta \end{aligned} \quad (69)$$

holds for $\xi = \xi_k, k \leq \tilde{K}$. We can rewrite (69) as the following matrix equation,

$$\mathbf{A}_{path} \mathbf{c}_\beta = \mathbf{y}_{path}, \quad |\beta| \leq p_2, \quad k \leq \tilde{K},$$

with the (k, β) -th entry $(\mathbf{A}_{path})_{k\beta} = \xi_k^\beta$, β -th entry $\mathbf{c}_\beta = \mathbf{i}^{|\beta|} b_\beta$, and k -th entry

$$(\mathbf{y}_{path})_k = \chi^{-1}(t_1, t_2, \xi_k, W) \left[\widehat{u}(t_2, \xi_k) - \widehat{u}(t_1, \xi_k) \exp\left((2\pi)^{-\frac{d}{2}} \sum_{|\alpha|=0}^{p_1} a_\alpha(\mathbf{i}\xi_k)^\alpha(t_2 - t_1)\right) \right].$$

By the assumption, \mathbf{A}_{path} is of full rank. Hence b_β can be determined uniquely. \square

In the multiplicative noise case, we present a pathwise identification result for the diffusion coefficients based on the known information about a_α and the increment of Brownian motion.

Proposition A.2. *Given $a_\alpha, |\alpha| \leq p_1$, and $W(t_2) - W(t_1)$ with $|t_2 - t_1| > 0$ sufficiently small (for a single trajectory), let $\mathcal{Q}_1 = \{\xi \in \mathbb{Z}^d : \widehat{u}_0(\xi) \neq 0\}$ satisfy*

$$|\mathcal{Q}_1| \geq \max\left(\sum_{k=0}^{\lfloor \frac{p_2}{2} \rfloor} \binom{2k + d - 1}{d - 1}, \sum_{k=0}^{\lfloor \frac{p_2 - 1}{2} \rfloor} \binom{2k + d}{d}\right), \text{ a.s..}$$

Suppose that \mathcal{Q}_1 is not located on an algebraic polynomial hypersurface of degree $\leq p_2$ consisting of only even-order terms or odd-order terms. Then the parameters are unique determined by the solution at two time points $u(t_1, \cdot), u(t_2, \cdot)$, and $W(t_2) - W(t_1)$.

Proof. We can choose the Fourier modes $\xi_k \in \mathcal{Q}_1$ with $k = 1, \dots, \tilde{K} \geq |\mathcal{Q}_1|$, and reformulate (11) and (12) as

$$\mathbf{y}_{even} = \mathbf{A}_{even} \mathbf{c}_{even}, \mathbf{y}_{odd} = \mathbf{A}_{odd} \mathbf{c}_{odd},$$

where $(\mathbf{A}_{even})_{k\beta} = \xi_k^\beta$, $(\mathbf{c}_{even})_\beta = \mathbf{i}^{|\beta|}(W(t_2) - W(t_1))b_\beta$ if $|\beta|$ is even, and $(\mathbf{A}_{odd})_{k\beta} = \xi_k^\beta$, $(\mathbf{c}_{odd})_\beta = \mathbf{i}^{|\beta|-1}(W(t_2) - W(t_1))b_\beta$ if $|\beta|$ is odd, and

$$\begin{aligned} (\mathbf{y}_{even})_k &= (2\pi)^{\frac{d}{2}} \log \left(\left| \frac{\hat{u}(t_2, \xi_k)}{\hat{u}(t_1, \xi_k)} \right| \right) - \sum_{|\alpha| \leq p_1, \alpha \text{ even}} a_\alpha(\mathbf{i}\xi)^\alpha (t_2 - t_1), \\ (\mathbf{y}_{odd})_k &= (2\pi)^{\frac{d}{2}} \text{Arg} \left(\left| \frac{\hat{u}(t_2, \xi_k)}{\hat{u}(t_1, \xi_k)} \right| \right) - \sum_{|\alpha| \leq p_1, \alpha \text{ odd}} a_\alpha(\mathbf{i}\xi_k)^\alpha (t_2 - t_1). \end{aligned}$$

Since $\mathbf{A}_{even}, \mathbf{A}_{odd}$ are of full ranks by the assumption and $W(t_2) - W(t_1) \neq 0, a.s.$, there exists a unique solution b_β . \square

A.3 Proof of Theorem 3.2 in additive noise case

Proof. In the additive noise case, according to Ito's isometry, it holds that

$$\begin{aligned} &\mathbb{E} \left[\left| \hat{u}(t_2, \xi) - \hat{u}(t_1, \xi) \exp \left((2\pi)^{-\frac{d}{2}} \sum_{|\alpha|=0}^{p_1} a_\alpha(\mathbf{i}\xi)^\alpha (t_2 - t_1) \right) \right|^2 \right] \\ &= \int_{t_1}^{t_2} \exp \left(2(2\pi)^{-\frac{d}{2}} \sum_{|\alpha| \leq p_1, \text{ even}} a_\alpha(\mathbf{i}\xi)^\alpha (t_2 - s) \right) |\hat{R}(\xi)|^2 ds \times \left| (2\pi)^{-\frac{d}{2}} \sum_{|\beta|=0}^{p_2} b_\beta(\mathbf{i}\xi)^\beta \right|^2. \end{aligned}$$

Notice that by our assumption

$$\tilde{F}(t_1, \xi, t_2) := \int_{t_1}^{t_2} \exp \left(2(2\pi)^{-\frac{d}{2}} \sum_{|\alpha| \leq p_1, \text{ even}} a_\alpha(\mathbf{i}\xi)^\alpha (t_2 - s) \right) |\hat{R}(\xi)|^2 ds > 0,$$

we can define

$$F(t_1, \xi, t_2) := \frac{\mathbb{E} \left[(2\pi)^d \left| \hat{u}(t_2, \xi) - \hat{u}(t_1, \xi) \exp \left((2\pi)^{-\frac{d}{2}} \sum_{|\alpha|=0}^{p_1} a_\alpha(\mathbf{i}\xi)^\alpha (t_2 - t_1) \right) \right|^2 \right]}{\tilde{F}(t_1, \xi, t_2)}.$$

Then the identification problem can be reformulated as

$$\begin{aligned} F(t_1, \xi, t_2) &= \left| \sum_{|\beta| \leq p_2} b_\beta(\mathbf{i}\xi)^\beta \right|^2 \\ &= \left[\sum_{|\beta| \leq p_2, \beta \text{ even}} \mathbf{i}^\beta b_\beta(\xi)^\beta \right]^2 + \left| \sum_{|\beta| \leq p_2, \beta \text{ odd}} \mathbf{i}^\beta b_\beta(\xi)^\beta \right|^2 \\ &= \sum_{|\beta|, |\tilde{\beta}| \leq p_2, \tilde{\beta}, \beta \text{ even}} \mathbf{i}^{|\beta|+|\tilde{\beta}|} b_\beta q_{\tilde{\beta}}(\xi)^{\beta+\tilde{\beta}} + \sum_{|\beta|, |\tilde{\beta}| \leq p_2, \tilde{\beta}, \beta \text{ odd}} \mathbf{i}^{|\beta|-|\tilde{\beta}|} b_\beta q_{\tilde{\beta}}(\xi)^{\beta+\tilde{\beta}}. \end{aligned} \quad (70)$$

Take $\xi_k \in \mathcal{Q}_1, k \leq \tilde{K}$ with $\tilde{K} \geq |\mathcal{Q}_1|$. It follows from (70) that

$$\mathbf{y}_{str} = \mathbf{A}_{str} \mathbf{c}_{str},$$

where $(\mathbf{y}_{str})_k = F(t_1, \xi_k, t_2)$, $(\mathbf{A}_{str})_{k\gamma} = \xi_k^\gamma, k \leq \tilde{K}, |\gamma| \leq 2p_2$ is even, and

$$(\mathbf{c}_{str})_\gamma = \sum_{|\beta|, |\tilde{\beta}| \text{ even}} \mathbf{i}^{|\beta|+|\tilde{\beta}|} b_\beta q_{\tilde{\beta}} + \sum_{|\beta|, |\tilde{\beta}| \text{ odd}} \mathbf{i}^{|\beta|-|\tilde{\beta}|} b_\beta q_{\tilde{\beta}} \quad (71)$$

with $\beta + \tilde{\beta} = \gamma$. By the assumption on \mathcal{Q}_1 , \mathbf{A}_{str} is of full rank and thus \mathbf{c}_{str} is uniquely determined. Since (71) is a quadratic function with respect to b_β , there exists at most $2^{\binom{p_2+d}{d}}$ isolated solutions, which are viewed as an equivalent class. Therefore, b_β is uniquely determined in the sense of an equivalent class. \square

It can be seen that, to obtain unique identification in the equivalent class, one can refine the assumption of \mathcal{Q}_1 in Theorem 3.2. In fact, to let Theorem 3.2 holds,

- in the additive noise case, it suffices to impose that Let $\mathcal{Q}_1 = \{\xi \in \mathbb{Z}^d | \widehat{R}(\xi) \neq 0\}$ satisfy

$$|\mathcal{Q}_1| \geq \sum_{k=0}^{p_2} \binom{2k+d-1}{d-1},$$

and suppose that \mathcal{Q}_1 is not located on an algebraic polynomial hypersurface of degree $\leq 2p_2$ consisting of only even-order terms.

- in the multiplicative noise case, it suffices to require that Let $\mathcal{Q}_1 = \{\xi \in \mathbb{Z}^d : \mathbb{E}\widehat{u}_0(\xi) \neq 0\}$ satisfy

$$|\mathcal{Q}_1| \geq \max \left(\sum_{k=0}^{p_2} \binom{2k+d-1}{d-1}, \sum_{k=0}^{p_2-1} \binom{2k+d}{d} \right),$$

and suppose that \mathcal{Q}_1 is not located on an algebraic polynomial hypersurface of degree $\leq 2p_2$ consisting of only even-order terms or odd-order terms.

Below we provide one simple example for possible multi-solutions in the equivalent class.

Example A.3. Let $d = 1$, $|\beta| \leq p_2 = 2$. Then from (70), we are solving the following system:

$$F(t_1, \xi, t_2) = b_0^2 + (-2b_2b_0 + b_1^2)\xi^2 + b_2^2\xi^4.$$

Let the number $\widetilde{K} > 0$ of Fourier modes be large enough (larger than 3 in this example). Then there exists a unique vector (x_1, x_2, x_3) such that $b_0^2 = x_1$, $-2b_2b_0 + b_1^2 = x_2$, $b_2^2 = x_3$. If the solution (b_0, b_1, b_2) exists for (70), then the number of the isolated solutions is at most 2^3 .

A.4 Proof of Theorem 3.3 in additive noise case

Proof. To verify (21), it suffices to show that there exists linear spaces V and V' with dimensions $L = \mathcal{O}(|\log \epsilon|^2)$ such that

$$\|e^{\mathcal{L}t}u_0 - P_V e^{\mathcal{L}t}u_0\|_{L^2(\Omega;H)} \lesssim \epsilon(1 + \|u_0\|_{L^2(\Omega;H)}), \quad (72)$$

and that

$$\|(I - P_{V'})u_{sto}\|_{L^2(\Omega;H)} \lesssim \epsilon(1 + \|u_0\|_{L^2(\Omega;H)}). \quad (73)$$

Here we denote $u_{sto}(t) = \sum_{k=1}^{\infty} \int_0^t e^{-(\lambda_k - \mu)(t-s)} q_k R_k \phi_k(x) dW(s)$ for convenience.

Consider the Galerkin approximation of $e^{\mathcal{L}t}$ with parameter \widetilde{M} ,

$$u_{ini, \widetilde{M}}(t, x) = e^{\mu t} \sum_{k=1}^{\widetilde{M}} c_k e^{-\lambda_k t} \phi_k(x)$$

and that of the stochastic convolution with parameter $M' \in \mathbb{N}$,

$$u_{sto, M'}(t, x) = \sum_{k=1}^{M'} \int_0^t e^{\mu(t-s)} e^{-\lambda_k(t-s)} q_k R_k \phi_k(x) dW(s).$$

We can take $\widetilde{K} \in \mathbb{N}^+$ such that $2\mu - \Re(\lambda_k) < 0$ for any $k \geq \widetilde{K}$. On the other hand, by the assumption, there exists $M_\epsilon \in \mathbb{N}^+$ such that $\sum_{k=M_\epsilon}^{\infty} \frac{1}{\Re(\lambda_k)} |q_k|^2 |R_k|^2 \leq \epsilon^2$.

By the Itô's isometry and the fact u_0 is \mathcal{F}_0 -measurable, we have that for $\widetilde{M} \geq \widetilde{K} + \epsilon^{\frac{2}{1-2\gamma}}$,

$$\mathbb{E}[\|u_{ini, \widetilde{M}}(t, \cdot) - e^{\mathcal{L}t}u_0\|^2] \leq \theta^2 \frac{\widetilde{M}^{1-2\gamma}}{2\gamma - 1}. \quad (74)$$

and that for $M' \geq \tilde{K} + M_\epsilon$,

$$\begin{aligned} \mathbb{E}[\|u_{sto,M'}(t, \cdot) - u_{sto}(t)\|^2] &= \mathbb{E}\left[\int_0^t \sum_{k=M'+1}^{\infty} e^{-2(\Re(\lambda_k) - \mu)(t-s)} |q_k|^2 |R_k|^2 \|\phi_k\|^2 ds\right] \\ &\lesssim \sum_{k=M'+1}^{\infty} \frac{1}{2\Re(\lambda_k)} |q_k|^2 |R_k|^2 \lesssim \epsilon^2. \end{aligned} \quad (75)$$

We first prove (72). Define

$$w_\epsilon^1(t) = \sum_{k=1}^{\tilde{M}} c_k \sum_{l=0}^{L_\epsilon} (-1)^l \frac{(\lambda_k t - \mu t)^l}{l!} \phi_k(x),$$

where $\tilde{M}, L_\epsilon > 0$, will be determined later. Then for each t , w_ϵ^1 sits in the linear space

$$V_1 = \text{span}\left\{\sum_{k=1}^{\tilde{M}} c_k (-1)^l \frac{(\lambda_k t - \mu t)^l}{l!} \phi_k(x), l = 0, 1, \dots, L_\epsilon\right\}.$$

By the Taylor expansion and Minkowski's inequality, as well as the independent increment of $W(\cdot)$, we have that

$$\begin{aligned} &\|w_\epsilon^1(t, \cdot) - e^{\mu t} \sum_{k=1}^{\tilde{M}} c_k e^{-\lambda_k t} \phi_k\|_{L^2(\Omega; H)}^2 \\ &\leq \left\| \sum_{k=1}^{\tilde{M}} c_k \phi_k(x) \sum_{l=L_\epsilon+1}^{\infty} (-1)^l \frac{(\lambda_k t - \mu t)^l}{l!} \right\|_{L^2(\Omega; H)}^2 \\ &\leq \sum_{k=1}^{\tilde{M}} \mathbb{E}[|c_k|^2] \left| \sum_{l=L_\epsilon+1}^{\infty} (-1)^l \frac{(\lambda_k t - \mu t)^l}{l!} \right|^2 \\ &\leq \sum_{k=1}^{\tilde{M}} \mathbb{E}[|c_k|^2] \frac{1}{[(L_\epsilon + 1)!]^2}, \end{aligned}$$

where we require that $\sup_{k \leq \tilde{M}} |\lambda_k - \mu| t \leq 1$, i.e., $t \in [0, \inf_{k \leq \tilde{M}} \frac{1}{|\lambda_k - \mu|}]$. It follows that for $t \in [0, \inf_{k \leq \tilde{M}} \frac{1}{|\lambda_k - \mu|}]$,

$$\|e^{\mu t} \sum_{k=1}^{\tilde{M}} c_k e^{-\lambda_k t} \phi_k - w_\epsilon^1(t, \cdot)\|_{L^2(\Omega; H)}^2 \leq \theta^2 \frac{\tilde{M}^{1-2\gamma}}{2\gamma - 1} e^{-2L_\epsilon}.$$

Letting $L_\epsilon = |\log(\epsilon)|$ and $\tilde{M} = \tilde{K} + \epsilon^{\frac{2}{1-2\gamma}}$, and using (74), we have that for $t \in [0, \inf_{k \leq \tilde{M}} \frac{1}{|\lambda_k - \mu|}]$,

$$\|e^{\mathcal{L}t} u_0 - w_\epsilon^1(t, \cdot)\|_{L^2(\Omega; H)} \lesssim \epsilon(1 + \|u_0\|_{L^2(\Omega; H)}). \quad (76)$$

For $t \in [\inf_{k \leq \tilde{M}} \frac{1}{|\lambda_k - \mu|}, T]$, by (18) and taking $\kappa = \sup_{k \leq \tilde{M}} |\log(|\lambda_k - \mu|)|/|\log(\epsilon)|$, there exists \mathcal{A}_L which is an approximation of $e^{\mathcal{L}t}$ such that $\|e^{\mathcal{L}t} - \mathcal{A}_L\|_{H \rightarrow H} \lesssim \epsilon$ with $t \in [t_0, T]$ such that $t_0 = \epsilon^\kappa$, and $L = C_{\mathcal{L}}(\kappa) |\log \epsilon|^2$. This implies that for any $t \in [\inf_{k \leq \tilde{M}} \frac{1}{|\lambda_k - \mu|}, T]$, there exists a linear space V_2 with dimension $L = C_{\mathcal{L}}(\kappa) |\log \epsilon|^2$ such that

$$\|e^{\mathcal{L}t} u_0 - P_{V_2} e^{\mathcal{L}t} u_0\| \lesssim \epsilon(1 + \|u_0\|_{L^2(\Omega; H)}).$$

This, together with (76), yields that for any $t \in [0, T]$, there exists a linear space V_3 containing $V_1 \cup V_2$ such that

$$\|e^{\mathcal{L}t} u_0 - P_{V_3} e^{\mathcal{L}t} u_0\| \lesssim \epsilon(1 + \|u_0\|_{L^2(\Omega; H)}). \quad (77)$$

Next, we prove (73). Define w_ϵ^2 by

$$w_\epsilon^2(t) := \sum_{k=1}^{M'} \int_0^t \sum_{l=0}^{L_\epsilon} (-1)^l \frac{((\lambda_k - \mu)(t-s))^l}{l!} q_k R_k \phi_k(x) dW(s)$$

with M', L_ϵ being determined later. It can be seen that w_ϵ^2 sits in the linear space

$$V_4 = \text{span} \left\{ \sum_{k=1}^{M'} (-1)^l \int_0^t \frac{((\lambda_k - \mu)(t-s))^l}{l!} q_k R_k dW(s) \phi_k(x), l = 0, 1, \dots, L_\epsilon \right\}.$$

Next, we use the Taylor expansion and Itô's isometry,

$$\begin{aligned} & \left\| w_\epsilon^2(t, \cdot) - \sum_{k=1}^{M'} \int_0^t e^{-(\lambda_k - \mu)(t-s)} q_k R_k \phi_k(x) dW(s) \right\|_{L^2(\Omega; H)}^2 \\ & \leq \left\| \sum_{k=1}^{M'} \int_0^t \sum_{l=L_\epsilon+1}^{\infty} (-1)^l \frac{((\lambda_k - \mu)(t-s))^l}{l!} q_k R_k \phi_k(x) dW(s) \right\|_{L^2(\Omega; H)}^2 \\ & \leq \sum_{k=1}^{M'} \int_0^t \left| \sum_{l=L_\epsilon+1}^{\infty} (-1)^l \frac{(\lambda_k - \mu)^l (t-s)^l}{l!} \right|^2 |R_k|^2 |q_k|^2 ds. \end{aligned}$$

By requiring that $\sup_{k \leq M'} |\lambda_k - \mu| t \leq 1$, i.e., $t \in [0, \inf_{k \leq M'} \frac{1}{|\lambda_k - \mu|}]$, and taking $L_\epsilon = |\log(\epsilon)|$, it follows that for $t \in [0, \inf_{k \leq M'} \frac{1}{|\lambda_k - \mu|}]$,

$$\begin{aligned} & \left\| w_\epsilon^2(t, \cdot) - \sum_{k=1}^{M'} \int_0^t e^{-(\lambda_k - \mu)(t-s)} q_k R_k \phi_k(x) dW(s) \right\|_{L^2(\Omega; H)}^2 \\ & \leq \sum_{k=1}^{M'} \int_0^t \frac{1}{[(L_\epsilon + 1)!]^2} |q_k|^2 |R_k|^2 ds \\ & \lesssim \sum_{k=1}^{M'} |q_k|^2 |R_k|^2 e^{-2L_\epsilon} t \lesssim \sum_{k=1}^{M'} |q_k|^2 |R_k|^2 \inf_{k \leq M'} \frac{1}{|\lambda_k - \mu|} e^{-2L_\epsilon} \lesssim \epsilon^2, \end{aligned} \quad (78)$$

where we also used the estimate $\inf_{k \leq M'} \frac{1}{|\lambda_k - \mu|} \leq \inf_{k \leq M'} \frac{1}{|\Re(\lambda_k) - \mu|} \lesssim \frac{1}{\Re(\lambda_k)}$ since $\Re(\lambda_{M'}) > 2\mu$ for M' large enough, and the fact that $\sum_{k=1}^{\infty} |q_k|^2 |R_k|^2 \frac{1}{\Re(\lambda_k)} \leq \sum_{k=1}^{\infty} |q_k|^2 |R_k|^2 \frac{1}{\Re(\lambda_k)^{1-\theta_1}} < \infty$.

We denote $t_1 = \inf_{k \leq M'} \frac{1}{|\lambda_k - \mu|}$ for simplicity. For $t \in [t_1, T]$, to obtain (73), we will show that there exist linear spaces V_5, V_6 such that

$$\|(I - P_{V_5}) \sum_{k=1}^{M'} \int_{t-t_1}^t e^{-(\lambda_k - \mu)(t-s)} q_k R_k \phi_k(x) dW(s)\|_{L^2(\Omega; H)} \lesssim \epsilon, \quad (79)$$

$$\|(I - P_{V_6}) \sum_{k=1}^{M'} \int_0^{t-t_1} e^{-(\lambda_k - \mu)(t-s)} q_k R_k \phi_k(x) dW(s)\|_{L^2(\Omega; H)} \lesssim \epsilon. \quad (80)$$

To verify (80) in $[t_1, T]$, by (18) with $L = C_{\frac{\epsilon}{2}}(\kappa) |\log(\epsilon)|^2$ and $\kappa = \sup_{k \leq M'} \log(|\lambda_k - \mu|/|\log(\epsilon)|)$, using the fact that $t - s \geq t_1 \geq \epsilon^\kappa$ and Itô's isometry, it holds that

$$\begin{aligned} & \left\| \sum_{k=1}^{M'} q_k R_k \int_0^{t-t_1} [e^{\frac{\epsilon}{2}(t-s)} - \mathcal{A}_{\frac{\epsilon}{2}}(t-s)] e^{\frac{\epsilon}{2}(t-s)} \phi_k dW(s) \right\|_{L^2(\Omega; H)}^2 \\ & \lesssim \sum_{k=1}^{M'} |q_k|^2 |R_k|^2 \epsilon^2 \frac{1}{\Re(\lambda_k)} \lesssim \epsilon^2. \end{aligned}$$

This implies that we can take the linear space V_6 generated by

$$\sum_{k=1}^{M'} q_k c'_l(z_l + \frac{1}{2}\mathcal{L})^{-1} \int_0^{t-t_1} e^{-z_l(t-s)} e^{\frac{\epsilon}{2}(t-s)} dW(s) \phi_k, |l| \leq L,$$

where $c'_l, z_l \in \mathbb{C}$, such that (80) holds.

To verify (79) in $[t_1, T]$, using Itô's isometry, by change of variables and the boundedness of $e^{\mathcal{L}(\cdot)}$, we obtain that for $\theta_1 \in (0, 1)$,

$$\begin{aligned} & \left\| \sum_{k=1}^{M'} q_k R_k \int_{t-t_1}^t [e^{-\frac{\epsilon}{2}(t-s)} - I] e^{-\frac{\epsilon}{2}(t-s)} \phi_k dW(s) \right\|_{L^2(\Omega; H)}^2 \\ & \lesssim \sum_{k=1}^{M'} \frac{|q_k|^2 |R_k|^2}{\Re(\lambda_k)} (e^{-\Re(\lambda_k)t_1} - e^{-2\Re(\lambda_k)t_1}) \lesssim \sum_{k=1}^{M'} \frac{|q_k|^2 |R_k|^2}{\Re(\lambda_k)^{1-\theta_1}} t_1^\theta. \end{aligned}$$

Here we take $M' \geq M_\epsilon$ large enough such that $\Re(\lambda_{M'})^{-\theta_1} \leq \epsilon^2$, and use the assumption that $\sum_{k=1}^\infty \frac{|q_k|^2 |R_k|^2}{\Re(\lambda_k)^{1-\theta_1}} < \infty$. As a consequence, we can take V_5 generated by $\sum_{k=1}^{M'} q_k R_k \int_{t-t_1}^t e^{\frac{\epsilon}{2}(t-s)} dW(s) \phi_k$ such that (79) holds.

Combining (79)-(80), and (78) together, we have that (73) holds for $t \in [0, T]$. □

B Some proofs in Section 4

B.1 Proof of Lemma 4.2

Proof. Notice that for any $i = 1, \dots, I$, we have

$$\begin{aligned} & \sum_{k=1}^K a_k \int_0^{t_i} \mathbb{E}[F_k(s, x)] ds + \mathbb{E}[u(0, x)] - \mathbb{E}[u(t_i, x)] \\ & = \sum_{k=1}^K (a_k - a_k^*) \int_0^{t_i} \mathbb{E}[F_k(s, x)] ds + \sum_{k=1}^K a_k^* \int_0^{t_i} \mathbb{E}[F_k(s, x)] ds + \mathbb{E}[u(0, x)] - \mathbb{E}[u(t_i, x)] \\ & = \sum_{k=1}^K (a_k - a_k^*) \int_0^{t_i} \mathbb{E}[F_k(s, x)] ds \end{aligned}$$

Hence, by the Cauchy-Schwarz inequality, we have

$$\begin{aligned} S_{\text{drift}}(\mathbf{a}) & \leq 2I^{-1} \cdot \sum_{i=1}^I \int_{\mathcal{D}} \left(\left(\sum_{k=1}^K (a_k - a_k^*) \int_0^{t_i} \mathbb{E}[F_k(s, x)] ds \right)^2 \right) dx \\ & \leq 2 \cdot \|\mathbf{a} - \mathbf{a}^*\|_2^2 \cdot I^{-1} \cdot \sum_{i=1}^I \int_{\mathcal{D}} \sum_{k=1}^K \left(\int_0^{t_i} \mathbb{E}[F_k(s, x)] ds \right)^2 dx \\ & \leq 2 \cdot \|\mathbf{a} - \mathbf{a}^*\|_2^2 \cdot \int_{\mathcal{D}} \sum_{k=1}^K \left(\int_0^T \mathbb{E}[F_k(s, x)] ds \right)^2 dx. \end{aligned}$$

□

B.2 Proof of Lemma 4.3

Proof. Since

$$\mathbb{E}[R_i^2(x, \mathbf{a}^*)] = \mathbb{E} \int_0^{t_i} \left(\sum_{j=1}^J \mathbf{b}_j^* G_j(s, x) \right)^2 ds,$$

we have that

$$\begin{aligned}
& S_{\text{diffuse}}(\mathbf{b}|\mathbf{a}) \\
&= I^{-1} \cdot \sum_{i=1}^I \int_{\mathcal{D}} \left| \mathbb{E} [R_i^2(x, \hat{\mathbf{a}})] - \mathbb{E} [R_i^2(x, \mathbf{a}^*)] + \mathbb{E} \int_0^{t_i} \left(\sum_{j=1}^J \mathbf{b}_j^* G_j(s, x) \right)^2 ds \right. \\
&\quad \left. - \mathbb{E} \int_0^{t_i} \left(\sum_{j=1}^J \mathbf{b}_j G_j(s, x) \right)^2 ds \right|^2 dx.
\end{aligned}$$

By the Cauchy–Schwarz inequality and the assumptions on the moment boundedness of features, we obtain

$$|S_{\text{diffuse}}(\mathbf{b}|\mathbf{a})| \leq C(\|\mathbf{a}\| + \|\mathbf{a}^*\|)^2(\|\mathbf{a} - \mathbf{a}^*\|^2) + C(\|\mathbf{b}\| + \|\mathbf{b}^*\|)^2\|\mathbf{b} - \mathbf{b}^*\|^2.$$

□

C Pseudo-code for Subspace Pursuit

We include the pseudo-code of Subspace Pursuit (SP) [18] for completeness.

Algorithm 2: Subspace Pursuit [18] for generating drift models

Input: Drift feature system $\mathbf{F} \in \mathbb{R}^{IM \times K}$ (35), $\mathbf{y} \in \mathbb{R}^{IM}$ (36) and $k \in \{1, \dots, K\}$.
Initialization: $\ell = 0$;
 $\bar{\mathbf{F}} \leftarrow$ column-normalization of \mathbf{F} ;
 $\mathcal{I}^0 = \{k \text{ indices corresponding to the largest magnitude entries in the vector } \bar{\mathbf{F}}^\top \mathbf{y}\}$;
 $\mathbf{r}^0 = \mathbf{y} - \bar{\mathbf{F}}_{\mathcal{I}^0} \bar{\mathbf{F}}_{\mathcal{I}^0}^\dagger \mathbf{y}$.
while *True* **do**
 Step 1. $\tilde{\mathcal{I}}^{\ell+1} = \mathcal{I}^\ell \cup \{k \text{ indices corresponding to the largest magnitude entries in the vector } \bar{\mathbf{F}}^\top \mathbf{r}^\ell\}$;
 Step 2. Compute $\bar{\mathbf{c}}^{(\ell+1)} = \bar{\mathbf{F}}_{\tilde{\mathcal{I}}^{\ell+1}}^\dagger \mathbf{y}$
 Set $\mathcal{I}^{\ell+1} = \{k \text{ indices corresponding to the largest elements of } \bar{\mathbf{c}}^{(\ell+1)}\}$;
 Step 3. Compute $\mathbf{r}^{\ell+1} = \mathbf{y} - \bar{\mathbf{F}}_{\mathcal{I}^{\ell+1}} \bar{\mathbf{F}}_{\mathcal{I}^{\ell+1}}^\dagger \mathbf{y}$;
 Step 4. **if** $\|\mathbf{r}^{\ell+1}\|_2 > \|\mathbf{r}^\ell\|_2$ **then**
 | Set $\mathcal{I}^* = \mathcal{I}^\ell$ and $\hat{\mathbf{c}}^* = \hat{\mathbf{c}}^{(\ell)}$, then **break**
 end
 else
 | Set $\ell \leftarrow \ell + 1$ and continue.
 end
end
Output: Indices of chosen features \mathcal{I}^* with $|\mathcal{I}^*| = k$ and reconstructed coefficients $\hat{\mathbf{c}}^* \in \mathbb{R}^K$ with $\text{supp}(\hat{\mathbf{c}}^*) = \mathcal{I}^*$.

References

- [1] D. C. ANTONOPOULOU, D. FARAZAKIS, AND G. KARALI, *Malliavin calculus for the stochastic Cahn-Hilliard/Allen-Cahn equation with unbounded noise diffusion*, J. Differential Equations, 265 (2018), pp. 3168–3211.
- [2] R. BALAN, B. G. BODMANN, P. G. CASAZZA, AND D. EDIDIN, *Painless reconstruction from magnitudes of frame coefficients*, Journal of Fourier Analysis and Applications, 15 (2009), pp. 488–501.

- [3] R. BALAN, P. CASAZZA, AND D. EDIDIN, *On signal reconstruction without phase*, Applied and Computational Harmonic Analysis, 20 (2006), pp. 345–356.
- [4] A. S. BANDEIRA, E. DOBRIBAN, D. G. MIXON, AND W. F. SAWIN, *Certifying the restricted isometry property is hard*, IEEE transactions on information theory, 59 (2013), pp. 3448–3450.
- [5] A. BECK AND Y. C. ELDAR, *Sparsity constrained nonlinear optimization: Optimality conditions and algorithms*, SIAM Journal on Optimization, 23 (2013), pp. 1480–1509.
- [6] J. BERG AND K. NYSTRÖM, *Data-driven discovery of PDEs in complex datasets*, Journal of Computational Physics, 384 (2019), pp. 239–252.
- [7] D. BLÖMKER AND A. JENTZEN, *Galerkin approximations for the stochastic Burgers equation*, SIAM J. Numer. Anal., 51 (2013), pp. 694–715.
- [8] L. BONINSEGNA, F. NÜSKE, AND C. CLEMENTI, *Sparse learning of stochastic dynamical equations*, The Journal of chemical physics, 148 (2018).
- [9] C.-E. BRÉHIER, J. CUI, AND J. HONG, *Strong convergence rates of semidiscrete splitting approximations for the stochastic Allen-Cahn equation*, IMA J. Numer. Anal., 39 (2019), pp. 2096–2134.
- [10] S. L. BRUNTON, J. L. PROCTOR, AND J. N. KUTZ, *Discovering governing equations from data by sparse identification of nonlinear dynamical systems*, Proceedings of the national academy of sciences, 113 (2016), pp. 3932–3937.
- [11] E. J. CANDÉS AND T. TAO, *Decoding by linear programming*, IEEE transactions on information theory, 51 (2005), pp. 4203–4215.
- [12] J. CHEN, M. K. NG, AND Z. LIU, *Solving quadratic systems with full-rank matrices using sparse or generative priors*, IEEE Transactions on Signal Processing, (2025).
- [13] J. CUI AND J. HONG, *Analysis of a splitting scheme for damped stochastic nonlinear Schrödinger equation with multiplicative noise*, SIAM J. Numer. Anal., 56 (2018), pp. 2045–2069.
- [14] J. CUI, J. HONG, AND Z. LIU, *Strong convergence rate of finite difference approximations for stochastic cubic Schrödinger equations*, J. Differential Equations, 263 (2017), pp. 3687–3713.
- [15] J. CUI AND L. SUN, *Quantifying the effect of random dispersion for logarithmic Schrödinger equation*, SIAM/ASA J. Uncertain. Quantif., 12 (2024), pp. 579–613.
- [16] G. DA PRATO AND J. ZABCZYK, *Stochastic equations in infinite dimensions*, vol. 44 of Encyclopedia of Mathematics and its Applications, Cambridge University Press, Cambridge, 1992.
- [17] R. D’AGOSTINO AND E. S. PEARSON, *Tests for departure from normality. empirical results for the distributions of b^2 and $\sqrt{b_1}$* , Biometrika, 60 (1973), pp. 613–622.
- [18] W. DAI AND O. MILENKOVIC, *Subspace pursuit for compressive sensing signal reconstruction*, IEEE transactions on Information Theory, 55 (2009), pp. 2230–2249.
- [19] A. DEBUSSCHE AND J. PRINTEMPS, *Numerical simulation of the stochastic Korteweg-de Vries equation*, Phys. D, 134 (1999), pp. 200–226.
- [20] C. DONG, G. XU, G. HAN, B. J. BETHEL, W. XIE, AND S. ZHOU, *Recent developments in artificial intelligence in oceanography*, Ocean-Land-Atmosphere Research, (2022).
- [21] D. L. DONOHO AND M. ELAD, *Optimally sparse representation in general (nonorthogonal) dictionaries via ℓ_1 minimization*, Proceedings of the National Academy of Sciences, 100 (2003), pp. 2197–2202.
- [22] M. DU, Y. CHEN, AND D. ZHANG, *Discover: Deep identification of symbolically concise open-form partial differential equations via enhanced reinforcement learning*, Physical Review Research, 6 (2024), p. 013182.

- [23] A. DUCOS, A. DENIZOT, T. GUYET, AND H. BERRY, *Evaluating PDE discovery methods for multiscale modeling of biological signals*, arXiv preprint arXiv:2506.20694, (2025).
- [24] J. FAN, L. KONG, L. WANG, AND N. XIU, *Variable selection in sparse regression with quadratic measurements*, *Statistica Sinica*, 28 (2018), pp. 1157–1178.
- [25] F. FLANDOLI, M. GUBINELLI, AND E. PRIOLA, *Well-posedness of the transport equation by stochastic perturbation*, *Invent. Math.*, 180 (2010), pp. 1–53.
- [26] B. FORNBERG, *Generation of finite difference formulas on arbitrarily spaced grids*, *Mathematics of computation*, 51 (1988), pp. 699–706.
- [27] A. GERARDOS AND P. RONCERAY, *Principled model selection for stochastic dynamics*, arXiv preprint arXiv:2501.10339, (2025).
- [28] W. W. HAGER AND H. ZHANG, *A new conjugate gradient method with guaranteed descent and an efficient line search*, *SIAM Journal on optimization*, 16 (2005), pp. 170–192.
- [29] ———, *A survey of nonlinear conjugate gradient methods*, *Pacific journal of Optimization*, 2 (2006), pp. 35–58.
- [30] M. HAIRER, *Solving the KPZ equation*, *Ann. of Math. (2)*, 178 (2013), pp. 559–664.
- [31] R. Y. HE, H. LIU, W. LIAO, AND S. H. KANG, *IDENT review: Recent advances in identification of differential equations from noisy data*, arXiv preprint arXiv:2506.07604, (2025).
- [32] R. Y. HE, H. LIU, AND H. LIU, *Group projected subspace pursuit for block sparse signal reconstruction: Convergence analysis and applications*, *Applied and Computational Harmonic Analysis*, 75 (2025), p. 101726.
- [33] Y. HE, S.-H. KANG, W. LIAO, H. LIU, AND Y. LIU, *Robust identification of differential equations by numerical techniques from a single set of noisy observation*, *SIAM Journal on Scientific Computing*, 44 (2022), pp. A1145–A1175.
- [34] Y. HE, H. ZHAO, AND Y. ZHONG, *How much can one learn a partial differential equation from its solution?*, *Found. Comput. Math.*, 24 (2024), pp. 1595–1641.
- [35] D. J. HIGHAM AND P. E. KLOEDEN, *An introduction to the numerical simulation of stochastic differential equations*, Society for Industrial and Applied Mathematics (SIAM), Philadelphia, PA, [2021] ©2021.
- [36] J. HONG AND L. SUN, *Symplectic integration of stochastic Hamiltonian systems*, vol. 2314 of *Lecture Notes in Mathematics*, Springer, Singapore, [2022] ©2022.
- [37] S. H. KANG, W. LIAO, AND Y. LIU, *Ident: Identifying differential equations with numerical time evolution*, *Journal of Scientific Computing*, 87 (2021), pp. 1–27.
- [38] H. KUNITA, *Stochastic flows and stochastic differential equations*, vol. 24 of *Cambridge Studies in Advanced Mathematics*, Cambridge University Press, Cambridge, 1990.
- [39] Y. LI AND J. DUAN, *A data-driven approach for discovering stochastic dynamical systems with non-Gaussian Lévy noise*, *Physica D: Nonlinear Phenomena*, 417 (2021), p. 132830.
- [40] W. LIU AND M. RÖCKNER, *Stochastic partial differential equations: an introduction*, Universitext, Springer, Cham, 2015.
- [41] Z. LONG, Y. LU, AND B. DONG, *PDE-Net 2.0: Learning PDEs from data with a numeric-symbolic hybrid deep network*, *Journal of Computational Physics*, 399 (2019), p. 108925.
- [42] M. LÓPEZ-FERNÁNDEZ, C. PALENCIA, AND A. SCHÄDLE, *A spectral order method for inverting sectorial Laplace transforms*, *SIAM J. Numer. Anal.*, 44 (2006), pp. 1332–1350.

- [43] Y. C. MATHPATI, T. TRIPURA, R. NAYEK, AND S. CHAKRABORTY, *Discovering stochastic partial differential equations from limited data using variational Bayes inference*, Computer Methods in Applied Mechanics and Engineering, 418 (2024), p. 116512.
- [44] D. A. MESSENGER AND D. M. BORTZ, *Weak SINDy for partial differential equations*, Journal of Computational Physics, 443 (2021), p. 110525.
- [45] T. T. NGUYEN, C. SOUSSEN, J. IDIER, AND E.-H. DJERMOUNE, *NP-hardness of ℓ_0 minimization problems: revision and extension to the non-negative setting*, in 2019 13th International conference on Sampling Theory and Applications (SampTA), IEEE, 2019, pp. 1–4.
- [46] A. PAZY, *Semigroups of linear operators and applications to partial differential equations*, vol. 44 of Applied Mathematical Sciences, Springer-Verlag, New York, 1983.
- [47] J. B. READE, *Eigenvalues of positive definite kernels. II*, SIAM J. Math. Anal., 15 (1984), pp. 137–142.
- [48] S. H. RUDY, S. L. BRUNTON, J. L. PROCTOR, AND J. N. KUTZ, *Data-driven discovery of partial differential equations*, Science advances, 3 (2017), p. e1602614.
- [49] G. SALINETTI AND R. J.-B. WETS, *On the convergence of closed-valued measurable multifunctions*, Transactions of the American Mathematical Society, 266 (1981), pp. 275–289.
- [50] W. SONG, S. JIANG, G. CAMPS-VALLS, M. WILLIAMS, L. ZHANG, M. REICHSTEIN, H. VEREECKEN, L. HE, X. HU, AND L. SHI, *Towards data-driven discovery of governing equations in geosciences*, Communications Earth & Environment, 5 (2024), p. 589.
- [51] R. STEPHANY AND C. EARLS, *Weak-PDE-LEARN: A weak form based approach to discovering PDEs from noisy, limited data*, Journal of Computational Physics, 506 (2024), p. 112950.
- [52] S. A. STOUFFER, E. A. SUCHMAN, L. C. DEVINNEY, S. A. STAR, AND R. M. WILLIAMS JR, *The american soldier: Adjustment during army life. (studies in social psychology in world war ii)*, vol. 1, (1949).
- [53] C. TANG, R. Y. HE, AND H. LIU, *WG-IDENT: Weak group identification of PDEs with varying coefficients*, arXiv preprint arXiv:2504.10212, (2025).
- [54] M. TANG, W. LIAO, R. KUSKE, AND S. H. KANG, *Weakident: Weak formulation for identifying differential equation using narrow-fit and trimming*, Journal of Computational Physics, 483 (2023), p. 112069.
- [55] M. TANG, H. LIU, W. LIAO, AND S. H. KANG, *Fourier features for identifying differential equations (fourierident)*, arXiv preprint arXiv:2311.16608, (2023).
- [56] T. TRIPURA AND S. CHAKRABORTY, *A sparse Bayesian framework for discovering interpretable nonlinear stochastic dynamical systems with gaussian white noise*, Mechanical Systems and Signal Processing, 187 (2023), p. 109939.
- [57] T. TRIPURA, S. PANDA, B. HAZRA, AND S. CHAKRABORTY, *Data-driven discovery of interpretable Lagrangian of stochastically excited dynamical systems*, Computer Methods in Applied Mechanics and Engineering, 427 (2024), p. 117032.
- [58] S. VOGEL, *A stochastic approach to stability in stochastic programming*, Journal of Computational and Applied Mathematics, 56 (1994), pp. 65–96.
- [59] H. XU, H. CHANG, AND D. ZHANG, *DLGA-PDE: Discovery of PDEs with incomplete candidate library via combination of deep learning and genetic algorithm*, Journal of Computational Physics, 418 (2020), p. 109584.
- [60] Z. ZHANG AND Y. LIU, *A robust framework for identification of PDEs from noisy data*, Journal of Computational Physics, 446 (2021), p. 110657.